ARCTIC SYNOPTIC ACTIVITY ASSOCIATED WITH SEA ICE VARIABILITY USING SELF-ORGANIZING MAPS

BY

CATRIN MARIE MILLS

DISSERTATION

Submitted in partial fulfillment of the requirements
for the degree of Doctor of Philosophy in Atmospheric Sciences
in the Graduate College of the
University of Illinois at Urbana-Champaign, 2014

Urbana, Illinois

Doctoral Committee:

Emeritus Professor John Walsh, Chair
Associate Professor John Cassano, University of Colorado, Boulder
Associate Professor Steve Nesbitt
Assistant Professor Zhuo Wang

Abstract

Relationships between synoptic activity and sea ice variability in the Arctic are studied using self-organizing maps (SOMs) to categorize observed weather patterns over the 1979-2010 period. The European Centre for Medium-Range Weather Forecasts (ECMWF) Re-Analysis (ERA-interim, or ERAI) provides the daily sea level pressures from which the SOMs are computed. Time series of frequencies and durations of synoptic weather patterns are correlated with two sea ice metrics, Fram Strait ice outflow and year-to-year changes in September pan-Arctic sea ice extent. When compared to teleconnection indices commonly associated with sea ice variability, the Arctic Oscillation (AO), North Atlantic Oscillation (NAO), and Arctic Dipole (AD), some SOM patterns correlate more strongly with sea ice metrics. For example, Beaufort High synoptic patterns are increasing in frequency in spring and summer and their spring frequencies are associated with ice loss. Icelandic Low patterns show opposing influences on sea ice from wind-forcing and thermal advection. The phase lags between the SOM occurrences and sea ice variability offer the potential for augmentation of other approaches to seasonal sea ice prediction. The ERA-interim SOM analysis is used to quantify how the Community Climate System Model, Version 4 (CCSM4) captures synoptic activity in the twentieth and twenty-first centuries. The model undersimulates patterns important for ice loss, such as broad high pressures over the continents and ice cover, and simulates strong storm track features at a higher-than-observed frequency. Large-scale teleconnection patterns, such as the AO and AD, are reasonably captured but there are spatial shifts in centers of action (which are associated with ice motion biases) and enhanced interannual variability relative to the observations. Relationships between synoptic activity and year-to-year changes in sea ice extent are not as prominent in the 20th century model experiment and further weaken in the 21st

century. Accounting for seasonal SLP biases in the model enhances SOM frequency-ice correlations, suggesting that the model captures closer-to-observed atmosphere-ice linkages when SLPs are reasonably simulated. Strong low pressures over the Arctic predominate over the ice-free central Arctic during summer and fall in the 21st century.

Acknowledgements

There are many people who deserved to be thanked; I will surely forget some. For my PhD (and general life and career) education, I'd like to thank my advisor, John Walsh. He is definitely a scientist that I try to model myself after. Bill Chapman pretty much taught me FORTRAN. He is a coder that I try to model myself after. I consider him a mentor (and buddy). I am so appreciative to all of the professors in our department, who have an open door policy. Thanks to Steve for his help throughout the years, from my first weather class to the WRF class and beyond. The WRF class increased my confidence as a coder, for which I am infinitely grateful. Thanks also go to Zhuo. She is a great dynamics teacher and has given me much helpful advice. I learned so much in Tropical. Thanks to Bob, Eric, and Donna for taking a chance on an unknown kid. I had never even taken an atmos class! I also have to thank Mak for my first dynamics course. It's where I first started to feel like I belonged in atmospheric sciences. I am also very appreciative to NCAR and Clara for introducing me to so many amazing scientists and mentors. Clara is another classic scientist, like John. Thanks to my ASP visiting grad student stint, I was able to meet Matt Higgins and John Cassano. Even though John C. travels all of the time, he has always been willing to make time to chat and discuss my research. It makes me very excited for my future in Boulder!

There were a lot of people who helped me get to UI. The most important is my family, especially my mom. She didn't have a chance at higher education but somehow instilled a rage for knowledge in me. Then there are the people who have been there for me for fun and everything else, like Sara, one of my greatest friends who I can always laugh with, and Allie, one of my greatest friends and accountability buddy (accountabilibuddy?). Then there's Xiaoying,

the best thing to happen to me in my whole life. We usually spend most of our time at the library, but somehow, it's always the best time. Oh, the places we'll go.

Contents

Chapter 1

Introduction

Arctic sea ice extent has rapidly decreased over the past two decades (e.g., Stroeve et al. (2012); IPCC, 2013), as shown in Figure 1.1. The cause of the ice retreat has been linked to many factors, including increased surface temperatures, changes in atmospheric circulation and associated wind forcing (e.g., Ogi and Wallace (2012)), influxes of warm ocean water (e.g., Shimada et al. (2006); Alexeev et al. (2013)), the ice-albedo feedback, and changing storm tracks (e.g., Screen et al. (2011)). The ice cover has also thinned (Kwok and Rothrock (2009); Laxon et al. (2013)). The recent thinning has made sea ice more mobile and thus more susceptible to winds associated with atmospheric synoptic patterns (Rampal et al. (2009)). Accordingly, the variability of the atmospheric circulation on daily to seasonal timescales is becoming increasingly important for sea ice (Asplin et al. (2009)). The goal of this study is to characterize atmospheric patterns associated with sea ice variability on daily to seasonal timescales.

While ocean currents play an important role in the long-term motion of sea ice, surface winds are the primary drivers of short-term sea ice motion. Several studies have used sea level pressure (gradient wind) data in attempts to improve upon the presently limited predictive skill

of summer sea ice (NRC (2012)). Ogi and Wallace (2012) showed that low level winds play an important role in determining summer sea ice retreat, and more specifically, that low-level winds contributed to the 2007, 2010, and 2011 September sea ice extent minima. Wu et al. (2012) also analyzed observed monthly mean low-level winds using a modified empirical orthogonal function (EOF) technique and found that the Arctic Dipole and Central Arctic patterns both play a role in sea ice loss, as both features contain pressure gradients conducive to advecting ice out of the Arctic Ocean into the North Atlantic. However, these studies used monthly mean atmospheric fields, which can average out crucial synoptic patterns that play a role in ice motion and deformation.

Other studies have focused more on relationships between sea ice minima and changing storm tracks over the last few decades, as opposed to wind variability. Screen et al. (2011) examined the role of mean cyclone activity on sea ice variability (1979 – 2009), in terms of sea ice motion and extent in the Arctic. They found that during years of large perennial September sea ice loss there were fewer storms over the central Arctic Ocean in late spring and early summer (Figure 1.2, adapted from Screen et al. (2011), their Figure 6). Also, there were more cyclones during years of ice gain, although the relationship was not linear. According to Screen et al. (2011), there appears to be no trend in late spring and early summer cyclone frequency.

Other earlier studies, however, have found an increasing trend in high-latitude cyclone frequency (e.g., McCabe et al. (2001); Zhang et al. (2004)). Specifically, McCabe et al. (2001) found an increase in cyclone frequency and intensity in the high-latitudes and a decrease in mid-latitude cyclone frequency from 1959 to 1997. These findings were corroborated by Zhang et al. (2004), who analyzed cyclone activity from 1948 to 2002 and found an increase in cyclone frequency in the Arctic during winter, spring, and summer. They also noted that cyclones

seen over the Arctic can have either local or mid-latitude origins and that complex spatial and temporal variability exists in cyclone activity. However, if cyclone activity is a primary determinant of the summer sea ice minimum extent, there should be discernible trends in cyclone activity over the past few decades.

While these analyses of storm tracks add to the understanding of sea ice variability, the broader range of synoptic patterns over the Arctic should also be important to sea ice variability through dynamic and thermodynamic forcing. For example, the Beaufort High pressure pattern has been identified as a key driver of the extreme sea ice retreat of 2007 (L'Heureux et al. (2008)). An assessment of synoptic variability—as opposed to storm track variability—relevant to sea ice requires novel methods of diagnostic analysis. EOFs, for example, are subject to the orthogonality constraint, which confounds physical/dynamical interpretation of a set of patterns (e.g., spatial relationships). While the use of storm tracks or cyclone frequency over monthly periods represents another novel approach, storm tracks are defined over timescales of weeks to months, and important transient features can be lost in the integration of daily data over these timescales (see Figure 1.2).

The atmospheric sciences community makes uses of GCMs in order to project future ice extent (e.g., IPCC AR5). In order for these model projections to be credible, they should simulate the atmospheric circulation on all timescales, as the atmospheric circulation determines temperature advection, ice motion, and upwelling, for example. Also, many models have difficulty simulating the observed negative sea ice trends (e.g., IPCC, 2013; see Figure 1.3, taken from Stroeve et al. (2012)) and even with an improvement upon CMIP3 models, the uncertainty in future ice extent has not been greatly reduced (Stroeve et al. (2012)). In the present study, CCSM4 (Gent et al. (2011)), one of the most widely used global climate models,

has been shown to reasonably represent the Arctic atmosphere (de Boer et al. (2011)) and Arctic sea ice state (Jahn et al. (2011)). de Boer et al. (2011) showed that the model captures the spatial patterns and timescales of various Arctic variables, such as temperature, sea level pressure (SLP), and cloud properties. However, large biases do exist in representation of SLP in the Arctic: a low pressure bias exists in all seasons. The corresponding under-simulation of sea level pressure over the Arctic Ocean is associated with overly strong simulated storm tracks, especially over the North Atlantic and with the penetration of Atlantic storms too far into the Arctic. Jahn et al. (2011) posits that the difficulty in producing high pressures over the Beaufort Sea creates errors in simulating ice motion. Later in the 21st century, model projections suggest that the storm tracks will shift farther northward with the shifting temperature gradients (Bengtsson et al. (2006)). As the 21st century Arctic is projected to be ice free by 2070, Arctic storms may become stronger (Simmonds and Keay (2009); Vavrus et al. (2011)). Comprehensive studies have examined the effect of 21st century ice losses on the atmosphere (e.g., Deser et al. (2010a)) and some show that storm tracks, such as the Aleutian Low become stronger (Higgins and Cassano (2009)).

Self-organizing maps (SOMs; Kohonen (2001)) offer a way to link synoptic patterns to various meteorological variables, to quantify synoptic pattern characteristics, and to compare synoptic activity between observations and present and future climates. The SOM analysis, an artificial neural network algorithm, provides a convenient way to look at high frequency spatial data, such as the multi-dimensional time series common in the atmospheric sciences. SOMs are increasingly employed in atmospheric science for their ability to reduce the dimensionality of data into representative maps of a given variable (daily mean sea-level pressure, for example). They have also been shown to better capture the frequency (temporal variance) and spatial

patterns than principal component analysis (PCA) (Reusch et al. (2005)). Cavazos (1999) and Hewitson and Crane (2002) first made use of SOMs to study extreme weather events and synoptic climatology, respectively.Cassano et al. (2006) expanded the use of SOMs to extreme weather events in the Arctic, such as high temperatures and high winds, that may play a role in coastal vulnerability.

This study utilizes SOMs to better quantify the associations between observed synoptic patterns and sea ice variability on seasonal timescales. The associations to be quantified are those between synoptic patterns and two sea ice metrics. The synoptic patterns and one of the sea ice metrics, Fram Strait outflow, span all seasons, not just the summer season, which has been the focus of several previous studies (e.g., Ogi and Wallace (2012); Screen et al. (2011); L'Heureux et al. (2008)). The use of daily atmospheric data is an integral and novel component to our study, as sea ice responds dynamically as well as thermodynamically to transient atmospheric patterns. Both types of responses are implicitly addressed here. It should be noted, however, that variations in dynamic and thermodynamic forcing are inextricably linked through temperature advection by surface winds. This study aims to add to knowledge of changing Arctic synoptic activity and its relationship to sea ice and to bridge cyclone climatologies to analyses of synoptic activity.

The specific objectives of this study are the following:

1. Quantify observed Arctic synoptic activity in terms of spatial patterns and trends in recent decades using SOM.

2. Investigate relationships between identified synoptic patterns and sea ice metrics, such as year-to-year changes in sea ice extent and Fram Strait outflow.

3. Explore how well CCSM4 captures observed Arctic synoptic activity and large-scale teleconnection patterns.

4. Compare 20th and 21st century relationships between CCSM4 synoptic activity and year-to-year changes in ice extent in both the 20 and 21st centuries, and identify how CCSM4 projects synoptic activity to change in the late 21st century

Chapter 2 describes the data used to achieve the objectives described above. Chapter 3 discusses the SOM methodology and the ERA-Interim Master SOM used throughout the study, in addition to a grouping of the SOM patterns and the seasonality of the synoptic patterns within the Master SOM. Results of exploring objectives (1) and (2) are discussed in Chapter 4, and objectives (3) and (4) results are discussed in Chapter 5. Chapter 6 provides a summary of the main findings and highlights the utility of tools, such as SOMs, in studying relationships between synoptic activity and processes affected by synoptic activity (e.g., ice motion).

Figure 1.1: Observed Pan-Arctic September ice extent

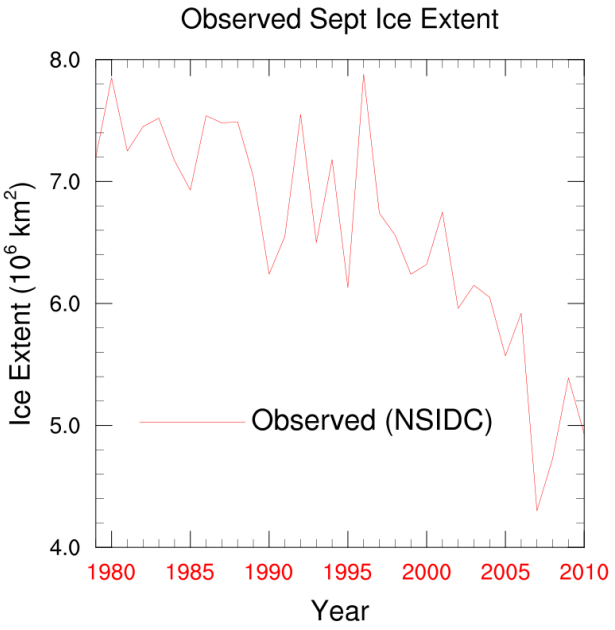

September observed sea ice extent (10^6km^2) from NSIDC (red line) for 1979 - 2010.

Figure 1.2: ILYs versus IGYs: SLP and Wind Stress

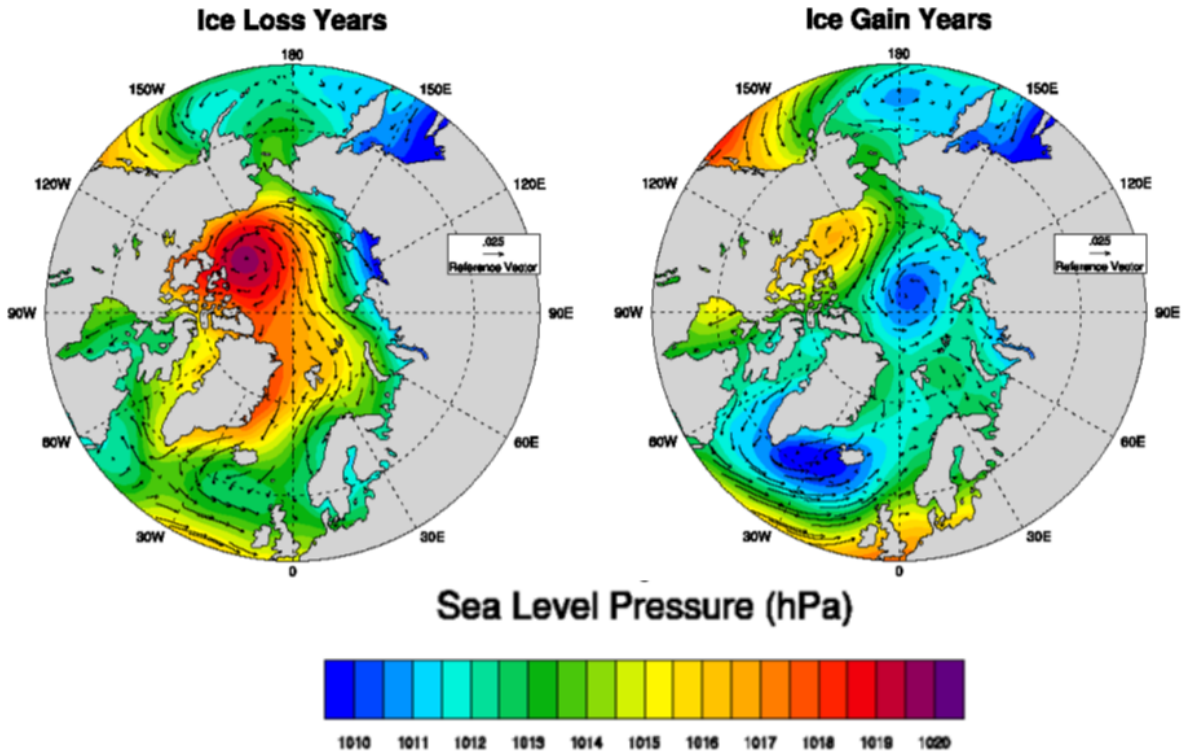

MJJ mean sea level pressure (colors, in hPa) and surface wind stress (vectors, in Nm-2) during ice loss years (defined as years during which there was a year-to-year loss of Sep ice area at least one standard deviation from the mean) and ice gain years (defined analogously for gains in ice area). The reference vector represents a wind stress of 0.025 Nm-2. Adapted from Screen et al. (2011), Fig. 6, using ERA-Interim monthly mean data.

Figure 1.3: Historical and Projected Sep Ice Extent: 1900 - 2100

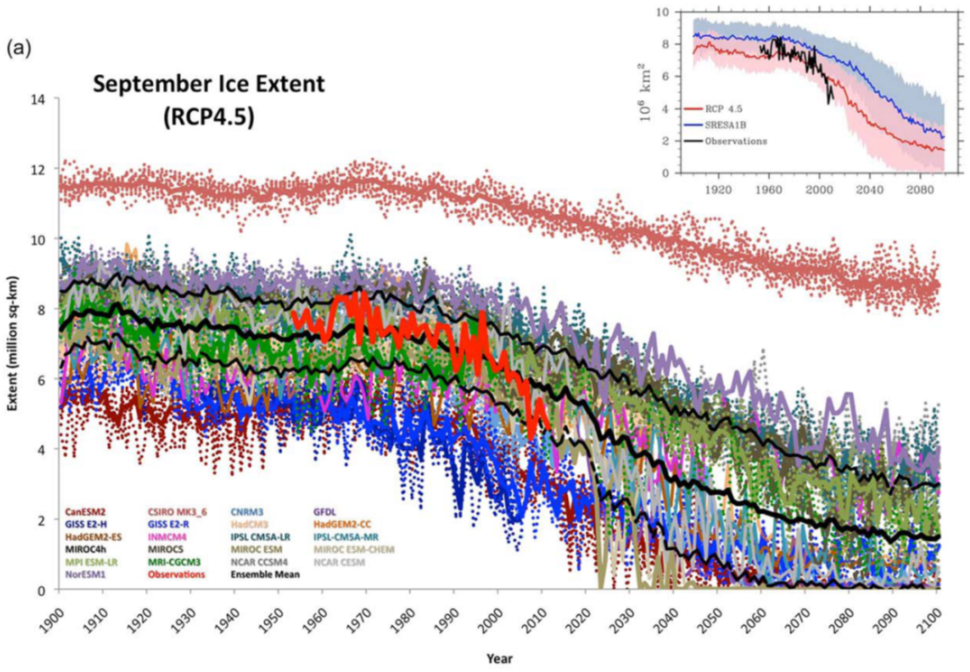

Projected September ice extent for various CMIP5 models using RCP 4.5 from 1900 to 2100. Figure 2(a) of Stroeve et al. (2012). Colors indicate the model used. Dotted lines indicate individual ensemble members, while the solid lines indicate the ensemble average. The solid red line indicates the observed ice extent. The solid black line represents the multi-model ensemble average, with thinner black lines on either side indicating the one standard deviation range. The top-right plot indicates the improvement from the SRESA1B scenario in CMIP3 experiments. The shaded colors represent one standard deviation multi-model ensemble mean spreads.

Chapter 2

Data

2.1 Atmospheric data

In order to represent synoptic patterns over the Arctic, daily averaged, six-hourly mean sea level pressure (SLP) data from the European Centre for Medium-Range Weather Forecasts (ECMWF) Re-Analysis (ERA-interim dataset, downloaded from the ECMWF Data Server) was used for the years 1979 – 2010. The ERA-interim dataset provides full coverage over the Arctic (as it is a global reanalysis), has a relatively fine spatial resolution of 1.5°, covers the entire modern satellite era (1979 – present), and has been shown to represent Arctic variables well in comparison with other reanalyses (Bromwich et al. (2007)) although it has been shown to have temperature biases below 850 hPa (Serreze and Barry (2005)). Screen et al. (2011) compared four reanalyses (ERA-interim, ERA-40, JRA-25, and NCEP-NCAR) for use in cyclone tracking and found that all showed similar interannual variability, further justifying its use in the present study.

The SLP data from ERA-Interim were regridded to a polar stereographic equal-area grid

to account for grid points converging toward the pole (i.e., to avoid the SOM analysis placing greater focus on SLP near the pole); this is analogous to cosine weighting in EOF analysis. Other variables used in the analysis of dynamic and thermodynamic effects of synoptic patterns on sea ice variability are daily averaged, six-hourly u- and v-winds at 10 meters and 2-meter temperature from 1979 – 2010. These are used to calculate temperature advection associated with each pattern.

Synoptic patterns identified by the SOM analysis are compared to three modes of atmospheric circulation variability, the North Atlantic Oscillation (NAO), Arctic Oscillation (AO), and Arctic Dipole (AD) in terms of their relationships to various sea ice metrics (Section 4.3). Time series of monthly NAO and AO indices were taken from the Climate Prediction Center (http://www.cpc.ncep.noaa.gov/products/precip/CWlink/pna/norm.nao.monthly.b5001.current.ascii and http://www.cpc.ncep.noaa.gov/products/precip/CWlink/daily_ao_index /monthly.ao.index.b50.current.ascii). The monthly AD time series is courtesy of Dr. Muyin Wang of NOAA's Pacific Marine Environmental Laboratory. For statistical analysis, these time series were averaged seasonally and annually (Oct – Sep, in order to capture each annual cycle from freeze-up to melt). The seasons are defined here on the basis of climatological monthly Arctic surface air temperatures (e.g., January-February-March, JFM, are the coldest months in the central Arctic) and are shifted by one month relative to the conventional seasonal definitions. In the present study, the following seasons will be used: JFM (winter), April-May-June (AMJ, spring), July-August-September (JAS, summer), and October-November-December (OND, winter).

2.2 Observational sea ice data

Two sea ice metrics time series were used to quantify interannual sea ice variability: annual (for the 12 months ending in September) Fram Strait ice outflow and year-to-year changes in September pan-Arctic sea ice extent, shown in Figure 2.1. The time series of sea ice extent minima in September was taken from National Snow and Ice Data Center (Fetterer et al. (aily), updated daily). Similar to Screen et al. (2011), year-to-year September sea ice extent changes (ΔSIE) were calculated because they highlight the variations of perennial (multi-year) sea ice. In comparison with the SIE, the time series of ΔSIE is less dominated by trend. An ice loss year (ILY) is defined as a year-to-year decrease in September minimum sea ice extent at least one standard deviation from the mean (year-to-year change). There are six ILYs: 1990, 1993, 1995, 1997, 2002, and 2007. An ice gain year (IGY) is defined analogously for a year-to-year increase in ice extent. Years 1980, 1992, 1994, 1996, and 2009 comprise IGYs. These metrics were then correlated to frequencies of occurrence of the SOM patterns (based on all years available, 1979-2010) shown in the following section. Fram Strait ice outflow data was taken from Kwok (2009), Figure 4, whose values are calculated using passive microwave brightness temperature and ice concentration data.

Figure 2.1: Observed year-to-year change in sea ice exent and Fram Strait Outflow

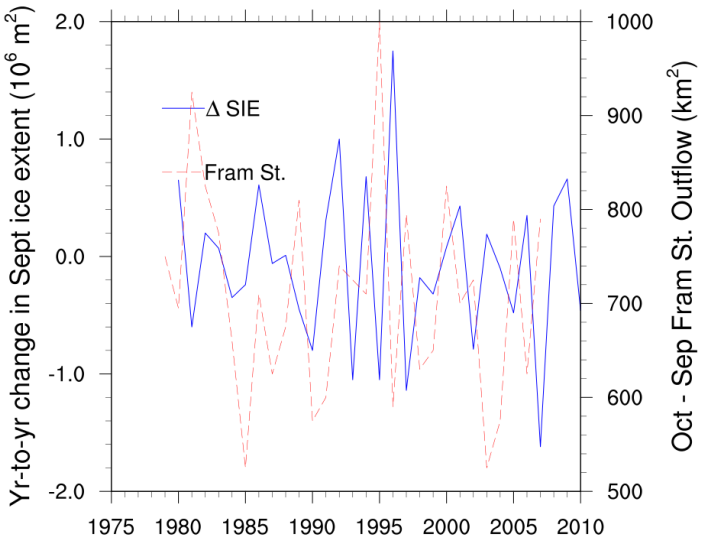

Year-to-year change in September sea ice extent (from NSIDC) is shown for 1980 – 2010 (blue solid line). Fram Strait area outflow is shown for Oct - Sep 1979 – 2007 (adapted from Kwok 2009, Fig. 4, represented by the dashed red line).

2.3 Model Output

CCSM4 is a fully coupled model with four model components (Gent et al. (2011)): atmosphere (Community Atmosphere Model Version 4, CAM4), land (Community Land Model Version 4, CLM4), sea ice (Los Alamos Sea Ice Model, CICE), and ocean (Parallel Ocean Model Version 2, POP2). Many features have been improved upon in the CCSM4 Arctic climate. For example, a parameterization called FREEZEDRY (Vavrus and Waliser (2008)) reduces positive low cloud biases in the Arctic in CAM4. Improved sea ice physics, such as ridging, and a melt pond parameterization, which improves Arctic snow/ice surface albedos, have been implemented into the CICE model. The CLM has a frozen soil scheme and considers snow properties, such as aging.

Twentieth century output from Ensemble #6 (the Mother of All Runs, or MOAR) is used as it has daily output for multiple variables. The twentieth century experiment is forced by transient greenhouse gas forcing from 1850 to 2005 and initialized with randomly-chosen years from a thousand year control run with 1850 radiative forcings. (Daily output of SLP was saved for Ensemble #4 and synoptic activity in both ensembles is found to be essentially identical.) Thirty-two years (model years 1974 to 2005) are analyzed so that the length of comparison periods is identical. Model years do not match year-by-year with the ERA-Interim reanalysis data; however, the model atmosphere is inherently stochastic and cannot be expected to reproduce various features at the same time in observations. It is thusly more important to compare temporal slabs of the same length and focus on comparing seasonal frequencies of synoptic patterns, rather than the timing of individual events, for example. Twenty-first century CCSM4 Ensemble #6 output is used from 2069 to 2100 (32 years total).

Ensemble #6 was initialized from the end of the 20th century experiment described above. The chosen ensemble is from the most extreme anthropogenic greenhouse gas forcing, representative concentration pathway 8.5 (RCP8.5), denoting a 8.5 W/m^2 radiative forcing anomaly (compared to preindustrial forcings) at the end of the century. The atmospheric data is on a 0.9° x 1.25° resolution (f09_g16, finite volume) grid, and ice data (which includes monthly fractional sea ice concentration) is on an approximately 1° grid. Analogous to the observed atmospheric data, spatial SLP anomalies are computed.

Chapter 3

Methodology

3.1 Classification of synoptic patterns: Self-organizing maps

The SOM analysis is an artificial neural network algorithm used here to reduce the dimensionality of daily spatial anomalies of SLP data into the representative synoptic patterns that span all seasons. Spatial anomalies are input into the SOM algorithm so that the training focuses on the SLP gradients (i.e., atmospheric circulation), as opposed to just the magnitudes of daily SLP fields. The analysis assumes no prior knowledge of the input data and preserves its probability distribution function (Kohonen (2001)). SOMs do have limitations, as they are computer assisted; the user must supply some parameters (as noted below). The user should make multiple master SOMs with varying parameters in order to find one that captures features the user deems important.

The SOM algorithm starts with randomly initialized set of weather patterns, or nodes, chosen by the user. Data for a randomly chosen daily SLP field, for example, are presented to each node within the Master SOM. The Euclidian distance between the data for a given day and

each node is calculated. The pattern with the shortest distance best represents the SLP field for a given day and is identified as the best matching unit (BMU). The BMU is then nudged to better represent the input data for the randomly chosen day, based on the learning rate, a user-set parameter. Neighboring nodes (weather patterns) are also nudged toward the input data field based on their distance from the BMU (which depends on the user-set parameter neighborhood radius). The training continues for more than 1,000,000 iterations, a parameter also set by the user. Sammon mapping (Sammon Jr (1969)) and quantization error allow the user to assess the stability and quality of the Master SOM that is produced. Frequencies of occurrence of the weather pattern matching each node are calculated by mapping each field within the dataset to its respective BMU.

The final product of the analysis is a Master SOM. Figure 3.1 shows the Master SOM trained on observed data, discussed in Chapter4. A Master SOM created from CCSM4 data is trained analogously and is discussed in Chapter 5. Adjacent nodes within the Master SOM are similar, offering an advantage over similar categorization techniques, such as EOFs or k-means partitions methods, for the purposes of studying transitions of weather patterns.

3.2 Master SOM

The Master SOM created from daily regridded ERA-interim SLP data, used as an example, is shown in Fig. 3.1. It depicts the synoptic patterns that occur from 50 to 90 °N over all days of all years. Winter patterns predominate in the top-left of the Master SOM, transitioning to more autumn-like patterns as one moves to the top-right. Spring patterns are on the bottom-left, summer patterns are on the bottom-middle, while patterns that occur during all seasons are in

the bottom-right. Overall, in Fig. 3.1, it is apparent that there is a higher pressure (i.e., fewer storms) over the central Arctic Ocean than subpolar regions and that storms penetrating into the Arctic with mid-latitude origins are most common in the Atlantic sector (e.g., broad high pressure patterns seen in the top portion of the Master SOM and Icelandic Lows on the right sides of the Master SOM), consistent with Zhang et al. (2004) and others.

3.3 Grouping of SOM patterns

The individual SOM weather patterns are grouped based on spatial correlations to facilitate the discussion, make statistical summaries of spatial and temporal changes of patterns, and to identify types of patterns that are related to sea ice loss or gain. Grouping also makes the trend and correlation statistics more robust (see Chapter 4). The grouping of the ERA-Interim Master SOM is discussed below, but grouping for the CCSM4 Master SOM is created analogously and discussed in Chapter 5.

For the grouping of the patterns in Figure 3.1, the spatial correlations between each pairing of patterns within a group were required to be at least 0.65, a threshold chosen by analyzing spatial correlations between all patterns within the Master SOM. This threshold is sufficiently high that patterns had to be spatially similar in order to be grouped yet low enough that there were no lone patterns. Sea ice correlations using grouped pattern frequencies are stronger than the means of correlations based on frequencies of single patterns within each group. Multiple groupings were tested using different methods (such as hierarchical agglomerative clustering, which builds and merges clusters, and groupings based on Euclidean distances) in order to examine the robustness of the groups. All groupings tested gave similar results in terms of

group trends and sea ice metric correlations. Figure 3.2 shows the Master SOM with the groups labeled; the lowest spatial correlation within a group is 0.69 (i.e., the lowest within-group correlation is 0.69 for the "Beaufort Highs/Eurasian Lows" and "Icelandic Lows/Fram Strait Outflow" groups).

The "High Pressure Bridges" group in the top-left of the Master SOM is characterized by a broad ridge extending across the ice cover and continents. The group in the top right, labeled "Eurasian Highs-Icelandic/Aleutian Lows" is spatially similar to the top-left group, but the broad ridge is weaker, especially over the ice cover. "Arctic Highs/Pacific Lows," in the middle-left of the Master SOM, shows strong highs over the central Arctic with shifting lows over the oceans. The bottom-right group shows similarities to the top-right group; however, the "Icelandic Lows/Fram Strait Outflow" patterns penetrate deeper into the Barents and exhibit pressure gradients conducive to wind-driven ice motion parallel to the Fram Strait. "Beaufort Highs/Eurasian Lows" is situated in the bottom-left of the SOM, characterized by Beaufort Highs of varying spatial scales and spatially shifting lows. Finally, in the bottom-middle is the "Weak Features" group, containing weaker pressure gradients and dominated by central Arctic lows.

Figure 3.1: ERA-Interim Master SOM

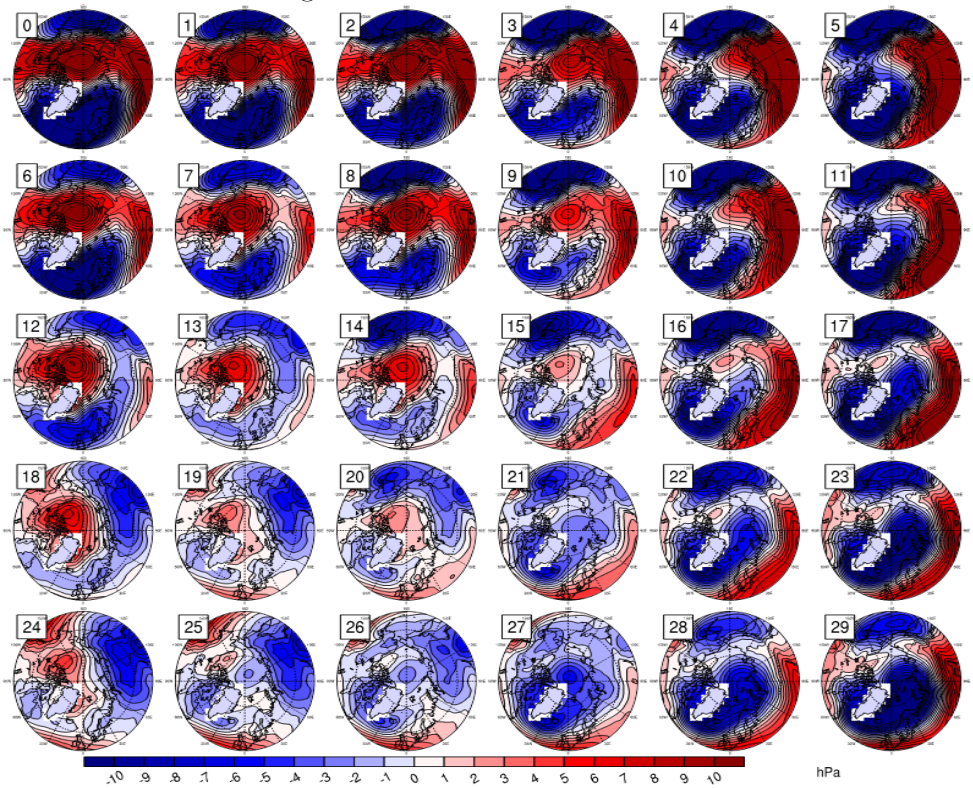

Master SOM of ERA-interim daily sea-level pressure spatial anomalies (hPa) from 1979 – 2010 (all days of all seasons).

Figure 3.2: ERA-Interim Master SOM Grouped

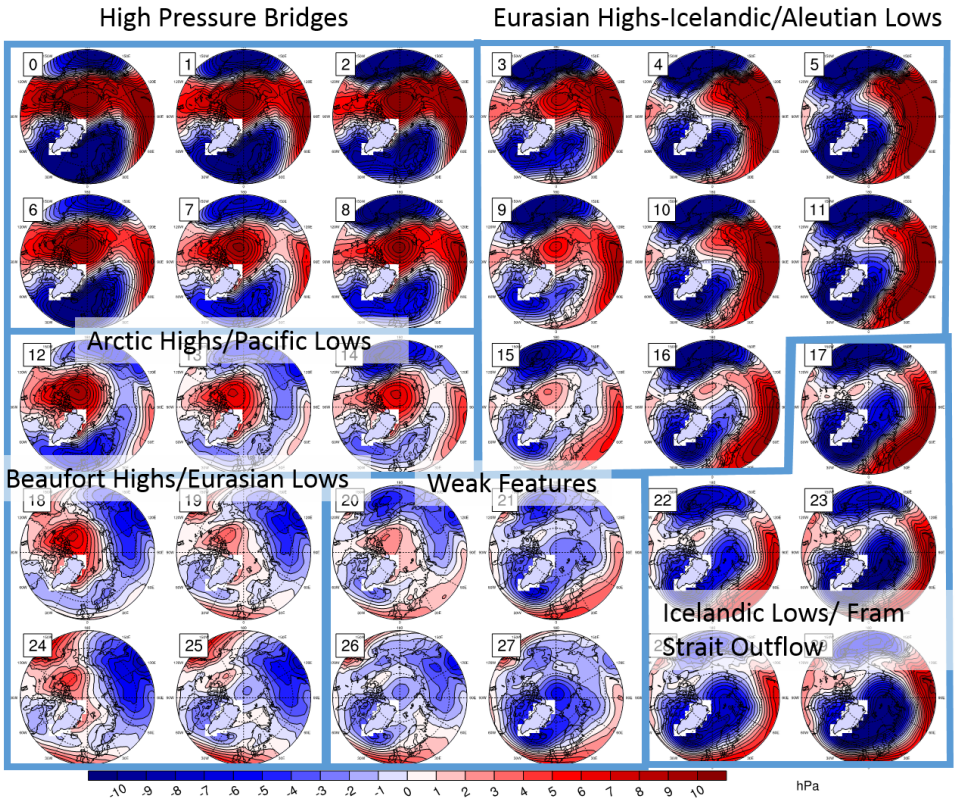

As in Figure 3.1 with bars and labels indicate groupings discussed in the text.

Chapter 4

Results I: Observed Arctic Synoptic Activity

4.1 Seasonality of SOM patterns

Figure 4.1 shows the mean frequencies per season for each SOM group labeled in Fig. 3.2. Most of the groups show notable seasonality, except for the "Icelandic Lows/Fram Strait Outflow" group, which occurs at least 6 days during each season. Most of the time series also display large interannual variability (Figure 4.2). Winter patterns with strong pressure gradients are the "High Pressure Bridges" and "Eurasian Highs-Icelandic/Aleutian Lows" groups, with high pressures over the continents (including the Siberian High) and over the ice cover (especially in the "High Pressure Bridges" group), occurring approximately 46 and 44 days during winter, respectively. This is consistent with cyclone climatologies, such as those of Zhang et al. (2004) and Serreze et al. (2001), who showed that cyclone centers predominate over the North Pacific

and North Atlantic during winter and that these storms contribute greatly to climatological low pressure signals. The Aleutian and Icelandic Lows, representing the storm tracks over the North Pacific Ocean and North Atlantic Ocean, respectively, are also present during winter. For spring, the high-pressure pattern centered near northern Canada and the Archipelago dominates in the "Arctic Highs/Pacific Lows" and "Beaufort Highs/Eurasian Lows" groups, consistent with a general weakening of the central Arctic's atmospheric circulation; the average frequencies of occurrence of these groups during spring are approximately 24 and 30 days, respectively. The patterns depicting high pressure over the continents also become less frequent, consistent with the increase in solar heating and the associated snow melt (Serreze and Barry (2005)). Also apparent is a slight northward shift of the low pressure features over the North Pacific and North Atlantic, likely owing to more storms of midlatitude origin propagating into the Arctic in winter than during summer (e.g., Zhang et al. (2004); Serreze et al. (2001)).

For summer a weaker circulation, in addition to northward shifts of the storm tracks (i.e., low pressure signals) and the summer cyclone maximum over the ice (Serreze and Barry (2005)), characterizes the "Weak Features" group, which occur on an average of ~44 days during the summer season. The SLP signal associated with enhanced cyclogenesis from Eurasia eastward to the Arctic Ocean and from Alaska to the Canadian Archipelago (Serreze et al. (2001)) is also present. The "Icelandic Lows/Fram Strait Outflow" group, occurring approximately 28 days in the fall (but at least 6 days during each season), shows the strengthening of the main pressure features present in winter (except over the ice cover). This strengthening is part of the transition into the "High Pressure Bridges" and "Eurasian Highs-Icelandic/Aleutian Lows" groups as the winter season starts. The patterns that are most common in autumn generally occur frequently in winter as well (as November and December are atmospherically winter months).

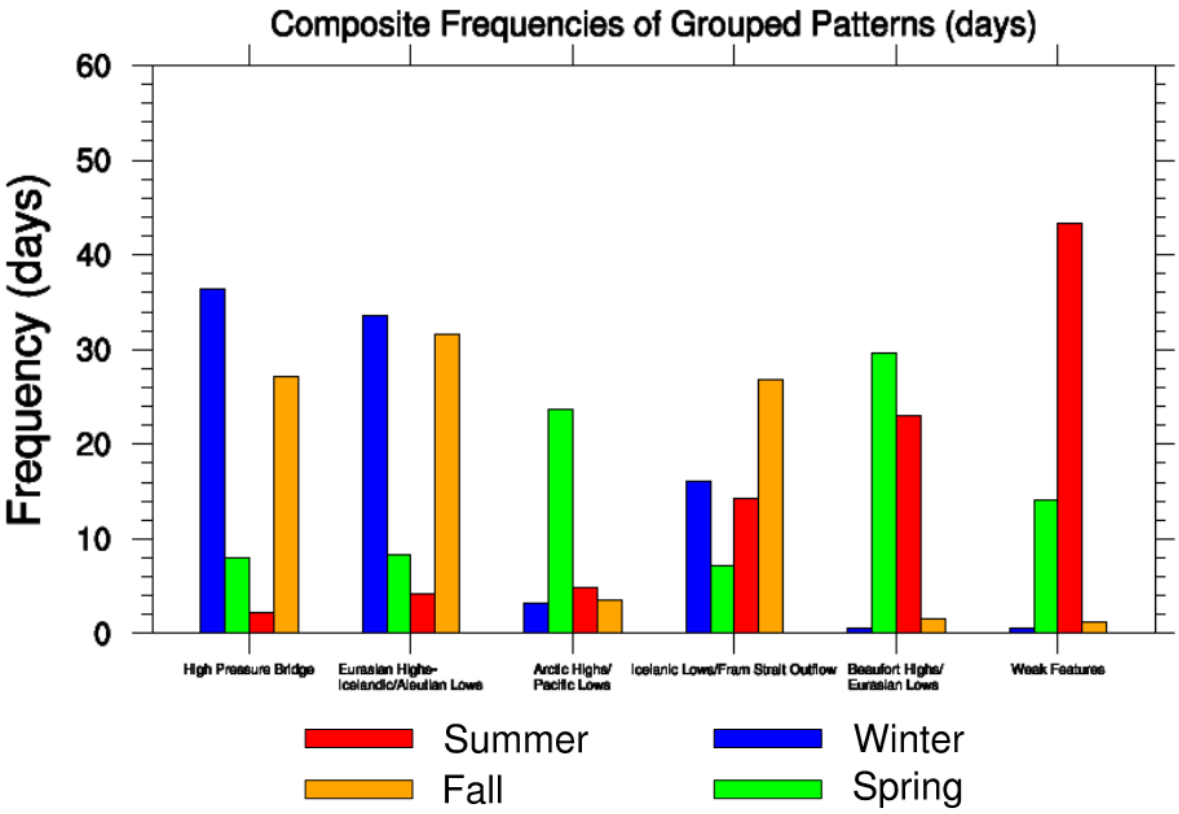

Figure 4.1: Composite frequencies for grouped SOM patterns

Seasonal composite frequencies (days) of grouped patterns (see Fig. 3.2) for JFM (blue), AMJ (green), JAS (red), and OND (orange).

4.2 Trends

Trends in frequencies of occurrence of grouped patterns are examined. In order to address variability amongst individual patterns within the given groups, time series and trends were also analyzed for individual SOM patterns in order to determine whether trends are consistent within a given group. Figure 4.2 shows the time series of frequencies of occurrence (dashed lines) for each group of patterns for each season (designated by color). Solid lines indicate the trendline for each time series. Table 4.1 shows the trends (expressed as the change in annual frequency of occurrence per decade, calculated using the trendline shown in Fig. 4.2). Trends appear to be most prominent during the summer season, while winter trends are weakest. The largest trend is ~±3 days per decade, which occurs for the "High Pressure Bridges", "Icelandic Lows/Fram Strait Outflow", and "Beaufort High/Eurasian Lows" groups.

The "High Pressure Bridges" group shows statistically significant negative trends in both summer and fall (-0.98 days at 95% statistical significance and -3.29 days per decade at 90% statistical significance, respectively). This group also shows an overall increase in winter of 1.18 days per decade, although the increase is not statistically significant at 90% confidence. The group labeled "Eurasian Highs-Icelandic/Aleutian Lows" shows a shift in winter and fall occurrences (see Fig. 4.2), decreasing by 1.73 days per decade in winter and increasing by 1.56 days per decade in fall (although the trends are not significant at 90% confidence). The seasonal shifts in trends of these two groups indicate a shift to stronger high pressure patterns over the sea ice during winter (i.e., a shift to more "High Pressure Bridges" type patterns) and an increase in Icelandic Low storm tracks penetrating into the Barents Sea during the fall (i.e., an increase in "Eurasian Highs-Icelandic/Aleutian Lows"), consistent with positive trends in

Arctic cyclone frequencies found in Zhang et al. (2004) and McCabe et al. (2001). However, direct comparisons to cyclone trends cannot be made as low pressures are present in all SOM patterns in Fig. 3.2.

Within the "High Pressure Bridges" group, only pattern 1 (see Fig. 3.2) exhibits a statistically significant trend at the 95% level in winter. Patterns 2 and 8 show a decrease of ~3 days and 1 day, respectively, while the other patterns within the group show an increase in frequency of up to 3 days. Considering that the patterns on the right-hand side (2 and 8) are relatively weaker in intensity than the patterns on the left-hand side of the group (0, 1, 6, and 7), this suggests that these broad high pressures are strengthening over the continents and the ice cover during winter and/or the Aleutian and Icelandic storm tracks are strengthening or penetrating farther poleward. As noted earlier, some studies have suggested poleward shifts of storm tracks have occurred in observations over recent decades (McCabe et al. (2001)). Supporting this idea is the overall decrease in the "Eurasian Highs-Icelandic/Aleutian Lows" group in winter. There is relatively little change amongst individual patterns in the "High Pressure Bridges" group during spring and summer (although the patterns rarely occur during the summer). During fall, pattern 0 decreases in frequency by ~7 days over the time period (not shown), contributing to this group's overall decrease in frequency during fall.

The "Arctic Highs/Pacific Lows" group, a predominantly spring pattern, shows a consistent annual decrease in occurrence during the spring and summer seasons of -1.33 and -1.26 days per decade, respectively (the summer trend is statistically significant at 90%). The "Icelandic Lows/Fram Strait Outflow" group shows positive trends in all seasons except winter; only the summer trend of 2.95 days per decade is statistically significant at 95%. The "Weak Features" group shows negative trends of up to 2.90 days per decade (in summer) in all seasons except

winter (0.18 days per decade). This could be associated with noted decreases in SLP over the Arctic (Walsh et al. (1996)); however, such trends are sensitive to the time period, as the Walsh et al. (1996) study analyzed times series with a shift from a negative to a positive AO phase.

The "Beaufort Highs/Eurasian Lows" group, a spring and summer pattern, shows positive trends of frequency during all seasons, with statistically significant trends during spring and fall of 3 days per decade (at 90% confidence) and 0.87 days (at 95% confidence), respectively. Individual pattern trends are prominent only in spring (patterns 18, 19, and 20) and fall (pattern 20), not shown, with the positive trends in spring indicating a shift to stronger Beaufort Highs, weaker Aleutian Lows, and/or stronger Eurasian Lows. Interestingly, climatological studies of the Beaufort High (Gleicher et al. (2011); Serreze and Barrett (2010)) have found little trend in vorticity metrics used to measure it. This may signal that the Beaufort High, itself, is not increasing in frequency but that this type of pattern, somewhat similar to the Arctic Dipole, has been persistent in recent years (e.g., Overland et al. (2012)).

Table 4.1: ERA-Interim SOM group frequency trends

Season	Winter	Spring	Summer	Fall
High Pressure Bridges	1.18	-0.53	-0.98**	-3.29*
Eurasia H- Ice/Al Lows	-1.73	0.03	0.38	1.56
Arctic H/ Pac Lows	0.29	-1.33	-1.26*	0.18
Ice Lows/ Fram St Outflow	-0.25	0.27	2.95**	0.83
Beaufort H/ Eurasia Lows	0.32	3.00*	1.80	0.87**
Weak Features	0.18	-1.44	-2.9	-0.15

Annual increase (decrease) of frequency of occurrence (days) for SOM groups per decade by season, indicated by positive (negative) numbers, of grouped patterns over the 1979 -2010 time period (days). Trends with one (**, ***) asterisk(s) indicates a statistical significance of 90% (95% and 99%, respectively) or greater.

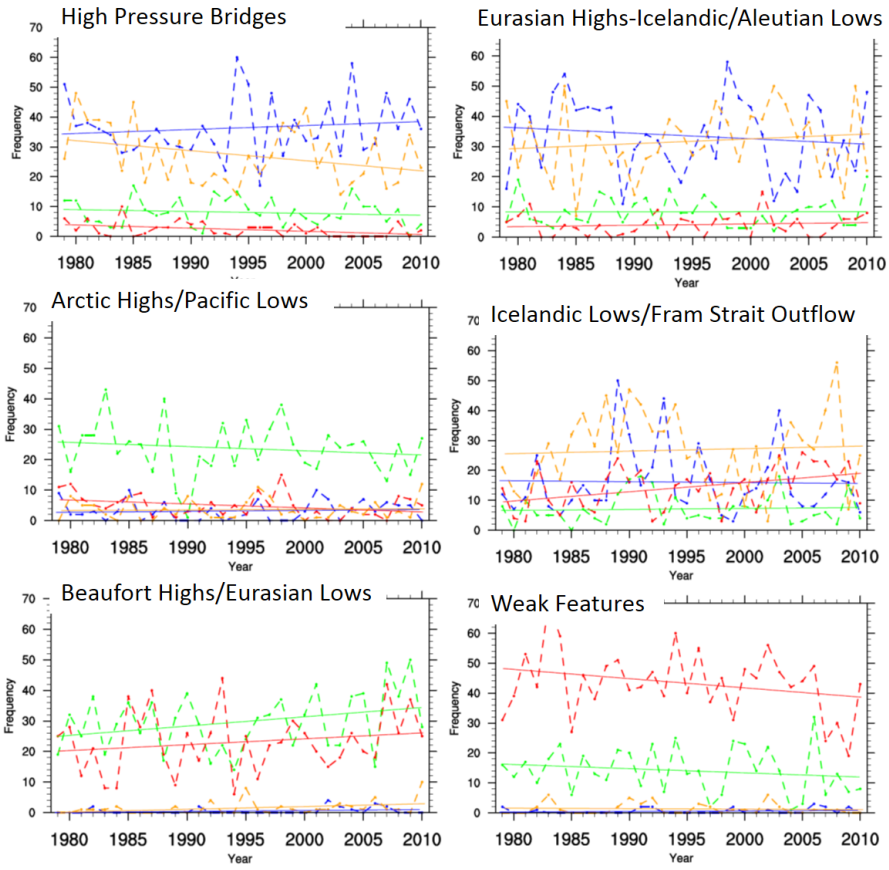

Figure 4.2: Grouped Patterns Frequency of Occurence Time Series

Time series of frequencies of occurrence (days) of grouped patterns (see Fig. 3.2) for JFM (blue), AMJ (green), JAS (red), and OND (orange) with respective trendlines.

4.3 Correlations to sea ice metrics

Table 4.2 shows correlations between SOM group frequencies of occurrence and sea ice metrics (Oct – Sep Fram Strait outflow and year-to-year ΔSIE). Also shown are correlations between time series of modes of atmospheric variability (AO, NAO, and AD) and the same sea ice metrics. Time series of Oct – Sep annual frequencies of occurrence are correlated to Oct – Sep Fram Strait outflow, and time series of seasonal (OND of year N-1; and JFM, AMJ, and JAS of year N) frequencies of occurrence are correlated to year-to-year changes (ending in year N) of September sea ice extent, ΔSIE so that lead-lag relationships can be examined. Correlations of detrended ice metrics to the SOM frequencies yielded similar results, indicating that correlations of the time series are not due to trends.

Screen et al. (2011) indicated that cyclone frequency in late spring-early summer plays a key role in preconditioning the ice for gain or loss. Because their study focuses specifically on cyclones, especially on the features captured by a cyclone-tracking algorithm, the importance of a "High Pressure Bridges" synoptic pattern may be overlooked. The "High Pressure Bridges" group shows a statistically significant (at 90%) correlation of 0.36 when Oct – Sep frequencies are correlated to Oct – Sep Fram Strait ice outflow; the group also shows a correlation of -0.37 (statistically significant at 95%) between winter (JFM) frequencies (preceding the September sea ice extent) and the year-to-year ΔSIE, i.e., the loss of perennial sea ice in the year ending in September. The observations also show a (non-statistically significant) increase of this pattern during winter (Fig. 4.2 and Table 4.1). Considering the group's pressure gradients east of Greenland (producing NE flow), both correlations provide quantitative support for this group's role in preconditioning the ice by advecting ice from the Eurasian coast and north of Greenland,

which is one of the locations of oldest sea ice (Maslanik et al. (2011)), out through the Fram Strait. The vacated sea along the Eurasian Coast quickly refreezes with young, thin, first-year ice that is more susceptible to a complete loss by summer melt.

The "Eurasian Highs-Icelandic/Aleutian Lows" group also shows significant correlations to Fram Strait outflow (-0.34) and year-to-year ΔSIE (-0.46) during AMJ (significant at the 90% and 99% level, respectively). Although this group is more prominent in winter and fall, it occurs about eight days on average during the spring (AMJ) season (Fig. 4.1). While it may seem inconsistent that some patterns correlate negatively with both changes in ice extent and with Fram Strait outflow, the details of the circulation and associated temperature advection with these patterns help to clarify the possible ice loss mechanism. Composite 2-m temperatures and 10-m winds associated with pattern 11 (a member of the "Eurasian Highs-Icelandic/Aleutian Lows" group), shown in Figure refWindTAdvexna, are conducive to wind forcing northward through the Fram Strait. Normally this would favor retention of sea ice in the Arctic basin. However, temperature advection associated with pattern 11 (Fig. 4.3) shows relatively strong warm advection in the region of the Fram Strait. The warm water and air transported northward can combine to melt sea ice, compensating for the inhibition of outflow associated with the southerly flow, an example of complex dynamic-thermodynamic mechanisms. While Arctic sea ice has decreased significantly during recent decades, this group does not show a prominent trend during spring (Fig. 4.2), ruling out changes in the frequency of this pattern type as the primary culprit in recent Arctic sea ice losses. Fig. 4.3 does not show quantitatively the relative importance of dynamics and thermodynamics, but it indicates that both factors contribute to the prominent correlations.

The only other group to correlate significantly with year-to-year change in ΔSIE is the

"Beaufort Highs/Eurasian Lows" group during AMJ, with a correlation of -0.50 at 99% statistical significance. The pressure gradients associated with the Beaufort High patterns in the group are consistent with shuttling ice into the Chukchi Sea (where it is affected by warmer Pacific water, Shimada et al. (2006)) and towards the Barents Sea and North Atlantic where it can melt. Many studies have suggested the 2007 record-setting September sea ice minimum can be attributed to a persistence of Beaufort Highs and Eurasian Lows, the so-called "dipole anomaly" (L'Heureux et al. (2008); Wu et al. (2012)), and these types of patterns are shown to have been increasing in recent decades (Fig. 4.2). 10-m winds overlayed onto 2-m temperature and temperature advection associated with pattern 24 of the "Beaufort Highs/Eurasian Lows" group are shown in Figures 6b and d, respectively. Strong positive temperature advection is located over the Bering Strait, the northern coast of Alaska and northeast Siberia. This circulation pattern is conducive to the transport of warm, salty Pacific water northward into the Arctic through Bering Strait, as well as warm air into the Arctic via advection and offshore (downslope) flow from the northern continental periphery. This pattern should also favor evacuation of sea ice away from the continental shelf regions near Siberia. The southward advection indicated in the eastern Arctic transports sea ice from the polar latitudes into the warmer North Atlantic water where it is efficiently melted. The group exhibits the most spatial similarities to the mean MJJ pressure pattern during ILYs (Screen et al. (2011), their Fig. 6, and adapted here in Fig. 1.2), occurring ~31 days during ILYs in AMJ and ~30 days during IGYs, with an overall mean frequency of occurrence of 30 days (Fig. 4.1). This suggests that other patterns and processes also play an important role in perennial ice variability.

The "High Pressure Bridges", "Eurasian Highs-Icelandic/Aleutian Lows", and "Beaufort Highs/Eurasian Lows" groups show, in some cases, stronger correlations to these sea ice metrics

than do modes of atmospheric circulation variability that are commonly used to diagnose sea ice variability: the AO and NAO (Stroeve et al. (2011); Rigor et al. (2002)), and the AD (Wu et al. (2012)). Correlations with indices of these patterns are shown in Table 4.2. The Arctic Oscillation and Arctic Dipole mean winter (JFM) indices show 90% statistical significance in their correlations of -0.31 (at 90%) and -0.58 (at 99%), respectively, highlighting the role of large-scale atmospheric variability on sea ice. Note that as the AD time series is defined, a negative phase corresponds to high pressure in the western Arctic and low pressure on the eastern side. We have shown that anticyclonic flow over the central Arctic Ocean is important to Fram Strait outflow, consistent with Ogi and Wallace (2012) and similar to the "Central Arctic" pressure pattern significantly correlated to SIE in Wu et al. (2012). Patterns with these anticyclonic signals are showing positive trends during winter with the "High Pressure Bridges" group and spring and summer with the "Beaufort High/Eurasian Low" groups.

These findings highlight the utility of SOMs to identify synoptic patterns that can be used to augment predictability of Arctic processes and variables. The SOM analysis allows utilization of daily atmospheric circulation fields and captures spatial variations of many synoptic patterns. The phase lags between the SOM frequencies and sea ice metrics, in conjunction with large-scale atmospheric modes of variability, offer the possibility of augmenting other approaches to seasonal ice prediction, via statistical methods.

Table 4.2: Correlations between grouped ERA-Interim SOM frequencies and ice metrics

		Yr-to-yr delSIE Correlations			
Circulation Pattern	Fram St. Out Corr	JFM	AMJ	JAS	OND
H P Bridges	0.36*	-0.37**	0.04	-0.15	-0.02
Eur Hs-Icelandic/Aleutian Ls	-0.34*	0.05	-0.46***	-0.09	-0.08
Arctic Hs/Pac Ls	0.13	0.07	-0.18	0	-0.02
Icelandic Ls/Fram Strait Out	0.06	-0.05	0.13	-0.12	0.09
Beaufort Hs/Eurasian Ls	-0.14	0.07	-0.50***	-0.28	0.03
Weak	0.04	-0.01	-0.22	0	-0.06
NAO	0.26	-0.24	0.26	-0.09	0.08
AO	0.28	-0.31*	0.09	0.10	0.20
AD	-0.58***	0.22	0.40**	0.34*	0.01

Correlations of Oct – Sep Fram Strait outflow and year-to-year change in Sep sea ice extent to frequencies of occurrence of grouped patterns, NAO, AO, and AD index time series. Oct – Sep correlations are shown for Fram Strait outflow, and seasonal correlations are shown for year-to-year changes in Sep sea ice extent. Correlations statistically significant at 90% or greater are bolded, while one (**, ***) asterisk(s) indicates a statistical significance of 90% (95% and 99%, respectively) or greater.

Figure 4.3: Winds overlayed on temperatures and temperature advection: Patterns 11 and 24

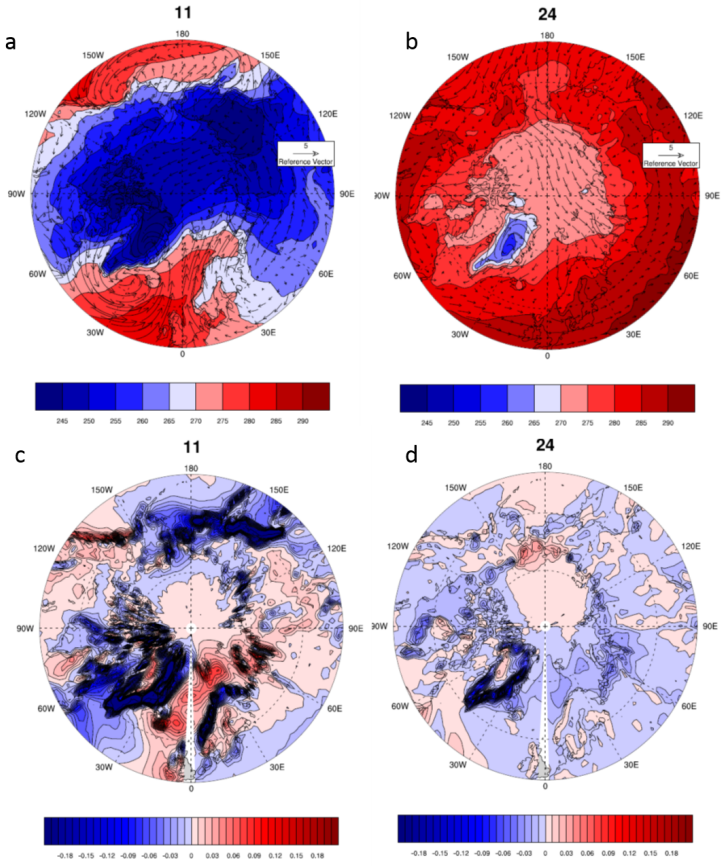

(Top) Composite 10-m winds (m/s) overlayed on 2-m temperature (K) in SOM patterns 11 (a) and 24 (b) from Fig. 3. (Bottom) Composite temperature advection calculated from 10-m winds and 2-m temperature fields (K/second) for patterns 11 (c) and 24 (d).

Chapter 5

Results II: Arctic Synoptic Activity in CCSM4: Present and Future Climates

5.1 Synoptic Activity in CCSM4: CCSM4 Present-Day Climate Vs. ERA-Interim

General circulation models (GCMs), such as CCSM4, are used for Arctic climate and climate change projections later in the 21st century. Stakeholders and communities are increasingly making use of these projections in decision-making in various fields, such as community relocation and the oil industry. Models used in these applications need to reasonably simulate the atmospheric synoptic-scale circulation, as this is important for ocean upwelling, temperature advection, and ice motion, amongst other processes. Bitz et al. (2002) discusses the significance

of models capturing high pressure systems over the Arctic in winter and low pressure features over the central Arctic during summer in order to simulate reasonable Arctic ice thicknesses. As discussed in Chapter 1, de Boer et al. (2011) show that CCSM4 has difficulties simulating high pressure over the Arctic and exhibits a low pressure bias, creating sea ice motion biases (Jahn et al. (2011)).

5.1.1 CCSM4 Ensemble Member Comparison

Examining multiple ensembles of the model is important, as slight changes in initial conditions produce different model projections (for example, Kay et al. (2011), discuss the importance of internal variability in CCSM4 in creating a large spread of ice extent losses amongst the 20th century ensemble members). Ensemble #6 is the main focus of this study, as daily output of many variables, such as temperature and downwelling longwave radiation, are available for this ensemble. Ensemble member #6 sea ice extent is shown in Figure 5.1 and begins to capture a more negative ice extent trend later in the 20th century. To ensure that ensemble member choice does not drastically change the synoptic results, other ensemble members for which daily output of SLP was saved for both the 20th and 21st centuries, ensemble members #4 and #5, were analyzed. Figures 5.38 and 5.39 show mean seasonal winter SLP for Ensembles #4 and #5. The main features are quite similar for the ensembles; for example, the Aleutian and Icelandic Low storm tracks have similar locations and intensities, although the low pressure centers in Ensemble #6 are slightly more intense (Figure 5.3). All of the ensembles fail to capture the strength of the observed winter Beaufort High (Figure 5.2). Ensemble #5, however, captures higher pressure extending from the Beaufort to the East Siberian Sea by ~5 mb.

During spring, Ensemble #6 better captures the Beaufort High-type pattern (Figure 5.5)

than do the other ensemble members (AMJ mean SLP for Ensemble #5 is shown in Figure 5.40). The ensembles are very similar in the other seasons with slight spatial variations; for example, Figures 5.41 and 5.42 show the mean JAS SLP for Ensembles #4 and #5. Both summer cyclone maximums near the pole are of similar magnitudes and only slightly more confined than the cyclone maximum in Ensemble #6 (Figure 5.10). Analogous analyses were conducted for ensemble members #4, 5, and 6 for the 21st century and yielded similar results.

Considering the investigation of the seasonal differences amongst the ensemble members, this shows that CCSM4 fails to capture the atmosphere-ice relationships in observations and that the SLP biases are largely systemic (i.e., the SLP features that are associated with the overall negative bias are consistent throughout the model), although some spatial variations do exist. Spatial features of teleconnection patterns (AO, NAO, and AD) were also compared and exhibited largely similar features (not shown). The underlying synoptics are largely similar amongst the ensemble members, as well. For example, both daily SLP fields of ensemble members #6 and #4 from the present-day CCSM4 climate were mapped to the ERA-Interim Master SOM and display nearly identical grouped synoptic pattern frequencies. Discussion will be limited to the CCSM4 Ensemble #6 as it has many variables with daily output. Examining ensemble members instead of ensemble averages also offers advantages (besides the ability to investigate daily output variables, such as temperature and longwave radiation fields), as the ensemble mean would dampen the internal variability associated with each ensemble.

5.1.2 Seasonal and Synoptic Patterns: ERAI Vs. CCSM4

Before mapping CCSM4 20th century SLP fields to the ERA-Interim Master SOM, a first sweep at assessing CCSM4's skill in simulating climatological mean SLP over the seasonal-synoptic

timescales is conducted. Seasonal and (selected) monthly means between the observations and CCSM4 are compared. Figure 5.2 shows Arctic winter (JFM) mean SLP from 1979 to 2010. High pressure exists over the continents, along with subpolar storm tracks over the oceans. In comparison, the CCSM4 mean JFM SLP (from model year 1974-2005), Figure 5.3, looks similar to Figure 5.2, although there are some important differences. The Icelandic low storm track penetrates too far northward and a local pressure maximum is non-existent over the ice cover in CCSM4, each contributing a mean SLP bias of ~-11 mb over the Greenland and Barents Seas and ~-10 mb spanning the Pacific side of the Arctic.

During spring (AMJ), ERA-Interim shows a relatively strong high pressure centered nearly over the Beaufort Sea (Figure 5.4). The pressure gradients on the north side of the high pressure are essentially parallel to the Transpolar Drift Stream (TDS). The Aleutian and Icelandic low storm tracks have also weakened, associated with the general weakening of Arctic atmospheric circulation as summer approaches (Serreze and Barry (2005)). Ensemble #6 from the 20th century CCSM4 run does not have a strong enough high pressure over the Beaufort (an approximately -6 mb bias) and shifts it farther south over northern Canada (Figure 5.5); however, CCSM4 is able to simulate pressure gradients oriented along the TDS. Examining observed monthly mean SLPs shows that the high pressure over the Beaufort is present in April (and also during JFM but slightly shifted), shown in Figure 5.6. CCSM4 does not simulate the high pressure in April (Figure 5.7) but starts to simulate it weakly in May (Figure 5.8).

ERA-Interim and CCSM4 mean JAS sea level pressure are shown in Figures 5.9 and 5.10, respectively. Consistent with de Boer et al. (2011), summer shows the weakest biases. CCSM4 is able to simulate the central Arctic Low but shifts it towards the Beaufort and strengthens it (producing a -4 mb bias). Recall that Bitz et al. (2002) found that simulating lows over

the central Arctic was important for ice motion. Screen et al. (2011) also noted that the low pressure in late spring-early summer was important for year-to-year ice gain. If the synoptic activity exhibits similar ice relationships to the observations, then the stronger shifted low plays a role in maintaining ice cover in the summer and could account for a weaker-than-observed ice trend.

The most prominent biases occur in the fall. ERA-Interim shows the strengthening high pressure over the ice cover and continents (Figure 5.11), while CCSM4 (Figure 5.12) fails to produce the high pressure over the ice cover (leading to a -14 mb bias) and simulates too strong of subpolar ocean storm tracks (with biases of -8 mb over the North Atlantic and -7 mb over southern Alaska).

In order to further quantify how well CCSM4 captures synoptic activity in the Arctic, including those synoptic patterns that correlate highly to sea ice variability, daily SLP patterns from present day CCSM4 were mapped to their corresponding BMUs (see Chapter 3 for a description) in the ERA-Interim Master SOM (Figure 3.2). There are multiple methods to go about such an analysis. An alternative method would be to create a Master SOM trained on both ERA-Interim and CCSM4 (analogous to methods used in Cassano et al. (2006), for example). This would create a map that would incorporate both datasets into training to represent the day-to-day Arctic SLP fields. The former method has been chosen since it considers ERA-Interim to be ground truth, so differences in CCSM4 are considered to be model biases, or errors. This method is preferred then since it focuses on the patterns already found to be important to ice variability in ERA-Interim (Chapter 4) so that a more direct comparison of biases can be discussed. Upon initial examination of Figures 5.14 through 5.19, CCSM4 does well in capturing the seasonality of the synoptic patterns.

Figure 5.14 compares the mean annual frequencies of occurrence for each season of the "High Pressure Bridges" group for the ERA-Interim and present-day CCSM4 climates, in addition to showing the SOM patterns that comprise each group (from Figure 3.2). CCSM4 undersimulates these broad Arctic high pressure patterns in all seasons. The most prominent bias is during fall, with CCSM4 simulating these patterns ~10 days less annually (statistically different from the ERA-Interim mean frequency of occurrence at 95% confidence). Considering that the model undersimulates these patterns by 6 days, and the mean high pressure spatial anomaly center (just poleward of the Beaufort) within the group is ~12 mb, the frequency bias contributes at least 1 mb to the seasonal mean SLP bias of ~-10 mb. In addition to frequency biases, biases of the CCSM4 fields that map to the "High Pressure Bridges" group also contribute to the overall SLP bias. To estimate the group's SLP bias contribution (i.e., intra-group bias), mean SLP fields for days mapped to their respective groups were calculated for CCSM4 and ERAI (not shown). The Beaufort High within the "High Pressure Bridges" in ERAI is ~1032 mb on average in fall, the corresponding Beaufort High is ~1022 mb in CCSM4 during fall. Considering that the "High Pressure Bridges" group occurs ~16 days during fall in the model, this contributes ~-2mb to the fall bias (to the overall Beaufort High bias of ~-10 mb during the fall). It should be noted that these are only estimates. The intra-group SLP bias contributes approximately double to the group bias than do the frequencies. This highlights that not only does CCSM4 produce too few strong high pressure patterns over the Arctic during fall, but also biases simulated highs toward weaker pressures.

Consistent with de Boer et al. (2011), the lowest bias is during summer, ~-2 days annually (not statistically different at 90%). Chapter 4 covered the importance of this type of pattern to both Fram Strait ice outflow and loss of perennial sea ice during winter; however, CCSM4

shows a 90% statistically significant bias of ~-6 days. This further highlights that CCSM4 undersimulates high pressure over the Arctic important for ice advection (de Boer et al. (2011)), although CCSM4 reasonably simulates March ice extent (Figure 5.13).

Another pattern important to ice loss and linked to warm air advection is the "Eurasian Highs/Icelandic-Aleutian Lows" group. Figure 5.15 shows the annual mean frequencies of occurrence by season for this group in ERA-Interim and CCSM4. Again, the model consistently undersimulates these patterns in all seasons. Although, this is a predominantly winter and fall pattern, the group's spring frequencies are linked to perennial ice loss. This group exhibits complex dynamical-thermodyanmical linkages, as it is linked to annual Fram Strait inflow and associated with prominent warm air advection through the North Atlantic. The largest bias of ~-10 days occurs during winter, contributing to the winter mean bias by at least -1 mb (the mean high pressure spatial anomaly is ~8 mb over the Beaufort). During winter, the differences in the mean ERAI and CCSM4 SLP fields associated with this group are not as prominent as for the "High Pressure Bridges" group. The Beaufort High pressure bias is ~-6 mb in CCSM4 and contributes ~-1.5 mb to the overall seasonal bias. The contribution of the under-simulation of these groups in CCSM4 and negative SLP biases within the group, itself, are roughly equal. Again, the smallest bias is during the summer months (~-2 days, not statistically significant at 90%).

Figure 5.16 shows the "Arctic Highs/Pacific Lows" group frequencies in the ERA-Interim and CCSM4 climates. This group weakly correlates to Fram Strait outflow and year-to-year changes in sea ice extent (Table 4.2). Again, this pattern is undersimulated in the CCSM4 present-day climate in all seasons (the winter bias is not statistically significant at 90%), especially in spring (~-12 days). This finding is also consistent with CCSM4's issues

in simulating Arctic high pressure patterns (de Boer et al. (2011)), contributing to the low pressure bias when comparing Figures 5.4 and 5.5.

The "Icelandic Lows/Fram Strait Outflow" group's frequencies of occurrence for both ERA-Interim and CCSM4 are shown in Figure 5.17. Interestingly, CCSM4 oversimulates this group during all seasons, especially fall (~22 day annual bias). The CCSM4 negative SLP bias for this group plays a larger role in the seasonal fall bias over the Beaufort (contributing ~-5 mb to the bias over this region during the fall). On the other hand, frequency biases contribute a larger role to the seasonal fall SLP biases over the Icelandic Low, as the mean SLP patterns for the "Icelandic Lows/Fram Strait Outflow" group are of similar magnitudes in ERAI and CCSM4. All seasons, except summer, display statistically significant biases at 99%. This group does not show prominent linkages to ice variability as this group only weakly and somewhat inconsistently correlates to Fram Strait outflow and year-to-year ice extent variability (Table 4.2). The far-northward penetrating Icelandic Lows displayed in the group are in agreement with a deeper-than-observed North Atlantic storm track suggested in de Boer et al. (2011).

"Beaufort Highs/Eurasian Lows" patterns correlated prominently to year-to-year changes in ice extent during spring (Table 4.2), and their frequencies of occurrence in CCSM4 and ERA-interim are shown in Figure 5.18. CCSM4 is able to predict this group linked to ice loss in spring, although it oversimulates it during AMJ (not statistically different at 90% than ERA-Interim frequencies) and winter (statistically significant at 99%). This oversimulation is associated with the northward shifted Eurasian Low (compare Figures 5.4 and 5.5). In all other seasons, CCSM4 under-predicts these patterns. Considering that these high pressure patterns over the Arctic are overall weaker than the "High Pressure Bridges" group, this signals that when the model does simulate these high pressures, they are at times too weak, in agreement

with the consistent low pressure bias compared to ERA-Interim.

The group that CCSM4 consistently over-simulates is the "Weak Features" group (Figure 5.19), overall dominated by central Arctic Lows and strong Aleutian Lows. This group weakly correlates the sea ice metrics, as shown in Table 4.2, likely associated with the weak pressure gradients within the group. Winter, spring, and summer biases of up to ~12 days during summer are all statistically significant at 99%.

In summary, these results show that CCSM4 overall captures the seasonality of patterns observed in CCSM4 but cannot consistently simulate high pressure patterns, such as the Beaufort High and broad Arctic ridges during the winter, important for ice motion (and temperature advection). CCSM4 produces stronger-than-observed storm tracks, and these low pressures are captured in terms of storms that penetrate too deep into the Arctic. Cassano et al. (2006) also noted that CCSM3 produces an elongated North Atlantic storm track in their SOM study of CMIP3 synoptic activity, showing that the NCAR model is consistent in this regard. These types of patterns are not prominently correlated to ice metrics. The model also oversimulates relatively weak low pressure features that predominate during summer and are not conducive to strong ice motion or advection. As shown in de Boer et al. (2011), CCSM4 shows the least SLP bias during summer.

The grouped CCSM4 frequencies of occurrence mapped to the ERA-Interim Master SOM (Figure 3.2) were correlated to year-to-year change in sea ice extent in CCSM4, shown in Table 5.1. Most correlations are weak, and prominent correlations displayed in the ERA-Interim climate (Table 4.2) no longer exist. The "Icelandic Lows/Fram Strait Outflow" group correlates at 0.34 (90% significant) to year-to-year September ice loss in winter and antecedent fall frequencies correlate to September ice gain at 0.32 (also significant at 90%). These correlations

seem spurious considering the year lag between the two time series. The only other group to correlate significantly (at 90%) to year-to-year changes in CCSM4 September ice extent is the High Pressure Bridge group, although it is, again, the group's fall frequencies for the year previous to the September ice extent (year N-1) that correlate significantly. The "Weak Features" group in CCSM4 shows the most prominent linkages in spring (with a correlation of -0.25), possibly associated with their high frequency of occurrence. The negative correlation, though, is counterintuitive to the findings of Screen et al. (2011), which showed that enhanced cyclonic activity over the central Arctic is linked to year-to-year ice gain.

5.1.3 CCSM4 Bias Correction

Weaker-than-observed atmosphere-ice linkages may be associated with overall negative SLP biases. To explore this, the mean seasonal SLP biases were subtracted from the CCSM4 output before being mapped to the ERAI Master SOM (Figure 3.2). It should be noted that although constant seasonal bias fields were subtracted from the input CCSM4 SLP fields, the frequencies of occurrence of do not change uniformly with the bias subtraction. Figure 5.20 shows the mean seasonal frequencies of occurrence of the "High Pressure Bridges" group when seasonal SLP bias corrections are applied to the CCSM4 ensemble member. CCSM4 now overpredicts the high pressure patterns in all seasons, except fall. The increases in frequencies are as high as 15 and 18 days in winter and spring (when compared to Figure 5.14). "Beaufort Highs/Eurasian Lows" are still undersimulated in all seasons, except summer (Figure 5.21). The "Weak Features" group patterns rarely occur after bias correction, except approximately 12 days in summer (Figure 5.22).

Mapping the bias-corrected model output to the ERAI Master SOM produces closer-to-

observed frequencies, so are the atmosphere-ice linkages also captured? Correlations between the bias-corrected annual frequencies (by season) and year-to-year ice variability in the CCSM4 ensemble were calculated analogously to Table 5.1. None of the frequency-ice correlations for patterns shown to correlate prominently to ice variability become robust at 90% significance, but they do become more prominent (not shown). For example, the "Eurasian High/Icelandic Lows" group correlations increase in magnitude from -0.13 to -0.21 in spring (compared to -0.46 in the observations; see Chapter 4). "Beaufort High/Eurasian Lows" correlations increase in magnitude from -0.08 to -0.10 in spring. These results suggest that SLP biases play a role in the weaker-than-observed interannual atmosphere-ice linkages. However, this finding does not hold true for the "High Pressure Bridges" group, for which the bias-corrected correlations increase from 0.01 to 0.28 in winter. This is counterintuitive to the Chapter 4 findings (correlation of -0.46 in the observational data), as the patterns have pressure gradients conducive to ice loss. If these strong high pressure patterns are linked to ice gain in the model, it suggests that other biases, such as the surface cold bias or underproduction of clouds may dampen the atmosphere-ice associations.

"High Pressure Bridges" patterns (linked to observed ice loss) are associated with lower-than-observed downwelling longwave radiation (by ~-60 W/m^2 over the central Arctic) in the model (compare Figures 5.23 for ERAI and 5.24 for CCSM4). Francis et al. (2005) find that observed downwelling longwave flux variability most highly correlates to perennial ice variability than to other variables, such as winds and shortwave fluxes. In regions where low clouds persist, downwelling longwave flux trends are controlled by an increase in cloud fraction and water vapor concentration (Francis and Hunter (2007)). de Boer et al. (2011) find that the CCSM4 has a cold bias in all seasons, likely linked to the underprediction of clouds in winter

and overproduction of clouds in summer. Considering that the "High Pressure Bridges" group correlates more prominently to ice variability when corrected for the negative SLP biases, the underpredicted downwelling longwave radiation (i.e., underprediction of clouds) may overwhelm the importance of this pattern to ice loss. Cloud biases also affect surface properties, such as ice albedo and thickness (Eisenman et al. (2007)). These processes (although likely intrinsically linked to atmospheric circulation) may be dominating year-to-year changes in ice extent in the CCSM4 present-day climate. Systemic biases may also be linked to interannual variability of the atmospheric circulation, which is intrinsically linked to processes that affect sea ice, such as temperature (via warm/cold air advection), surface winds, and ice age and motion. Ocean heat fluxes (Shimada et al. (2006)) and dynamical forcing (Ogi and Wallace (2012)) also affect ice variability and could play a role in the muted atmosphere-ice linkages. Another shortcoming of the model may be that interannual variability of the atmospheric circulation may not be adequately captured. Large-scale atmospheric teleconnections (the AO, NAO, and AD) in CCSM4 will be investigated in the following section, as it is most closely aligned to the present study.

5.1.4 Large-scale Atmospheric Variability in the Arctic

CCSM4 undersimulates SOM patterns associated with ice variability (e.g., "High Pressure Bridges"). The model's ability to capture large-scale relationships between the atmosphere and ice, such as the AO, NAO, and AD, is also investigated to identify if the model captures large-scale atmospheric teleconnection patterns. The AO is defined as the leading principal component (PC) of extended winter NDJFMA monthly mean SLP anomalies from 20-90 °N (Thompson and Wallace (1998)). Figure 5.25 shows the extended winter mean SLP anomalies

regressed onto the standardized time series associated with the EOF analysis (Figure 5.26). The AO accounts for ~21% of the extended wintertime SLP variance and the tripole pattern is apparent, with high pressure over the Arctic and low pressures centered in the subpolar regions (during the positive AO phase). Figure 5.27 shows the leading PC of winter SLP calculated analogously to the ERAI dataset. The model captures the overall tripole pattern and explains ~26% of the wintertime SLP variance, but the Arctic portion of the see-saw pattern is shifted toward the Eurasian-side of the Arctic. The subpolar signatures associated with the Aleutian Low are too strong by ~-3 mb and shifted toward the Gulf of Alaska. The signature associated with the Icelandic Low is more confined in the model and centered over western Europe. The CCSM4 AO index (Figure 5.28) shows more interannual variability than in observations, most prominent earlier in the time period of analysis, and also shows fewer strongly negative AO years than the observations.

The NAO can be defined as the leading PC of seasonal winter DJFM SLP anomalies over the Atlantic, 20-80 °N and 90 °W-40°E (Hurrell (1995)). Figures 5.29 and 5.30 show SLP anomalies regressed onto the standardized NAO index for each dataset. The model again shifts the centers of action eastward toward Eurasia in the case of the northern lobe (centered near Iceland in ERAI) and over western Europe in the case of the southern lobe. The associated time series of NAO index values for ERA and CCSM4 are shown in Figures 5.31 and 5.32. Again, the model shows enhanced interannual variability relative to the observations, especially earlier in the time period.

The AD pattern is also shifted in the model relative to the observations (Figure 5.33 for ERAI and Figure 5.34 for CCSM4). Overland et al. (2012) define the AD as the second leading principal component of individual monthly mean extended winter DJFM SLP anomalies

poleward of 70 °N. The AD explains ~15% of the wintertime SLP variance in the observations and ~12% in the model. The model shifts the western Arctic from over the Beaufort to over the Atlantic sector. This is likely associated with the model's under-simulation the Beaufort High and over-simulation Icelandic Low-type patterns, shifting the center of action. The model, however, does capture pressure gradients parallel to the TDS, which is what has made the AD a focus of Arctic ice studies in recent decades (e.g., Overland et al. (2012) and Wu et al. (2006)). The standardized time series for the ERAI dataset and CCSM4 output are shown in Figures 5.35 and 5.36. Examining the last few years of the AD time series for the model shows a predominantly negative phase, consistent with Figure 5.1, which shows a steeper negative ice extent trend in the ensemble since around the model year 2000. This suggests that the model does capture some atmosphere-ice connections, but are these consistent (i.e., coherent in time)?

Correlations between the described teleconnection indices and year-to-year changes in September sea ice extent in the CCSM4 ensemble member (Ensemble 6) are shown in Table 5.2. In general, the model correlations are weaker than in the observations (Table 4.2), except in spring for the case of the Arctic Dipole, correlating at 0.55 at 99% significance. The correlation for this month is stronger than observations and is likely associated with SLP biases over the Beaufort, contributing to an AD-like signal in spring (Figure 5.5). The most prominent correlations for the AO are in winter (-0.22)–consistent with observations (Table 4.2)– although none of the correlations are statistically significant at 90% or above.

Overall, the model's linkages between wind and ice are not coherent. This draws attention to the importance of interannual variability of the atmospheric circulation on ice variability. CCSM4 captures the overall ocean circulation patterns associated with the AO, shown in Figure 5.37, taken from Figure 9 of Jahn et al. (2011), but the anticyclonic circulation is shifted in

the model. The negative AO phase is associated with a strengthened Beaufort gyre in winter (bottom of Figure 5.37) in both the observations and the model, but the circulation patterns in the model are consistent with a large portion of ice being transported from along the Eurasian coast (in the Laptev Sea) toward the Canadian Archipelago; this would have little effect on ice extent (considering only mechanical effects on the ice field and without considering the effect of ice fracturing). On the other hand, the observed ice motion field associated with a negative AO phase shows a clear TDS pattern conducive to shuttling ice toward the Fram Strait form the Laptev Sea eastward. Slight spatial variations of leading modes of variability could have drastically different effects on ice fields. The model also shows more interannual variability of the teleconnection patterns. Recent studies have shown that the persistence of teleconnection patterns, such as the AD (e.g., Overland et al. (2012)), could be associated with the recent trends in September ice loss and even Arctic-midlatitude weather linkages. The SOM frequencies comprise the synoptic activity, which is enveloped by these teleconnection patterns. For example, mean frequencies of occurrence of SOM groups were calculated for the top five negative AO years in the observations and model. The composite frequencies are prominently different (not shown), with stronger high pressures associated with negative AO years in the observations. This suggests that the model's systemic bias (e.g., negative SLP bias) and enhanced large-scale atmospheric interannual variability contribute, at least partially, to the weaker-than-observed synoptic linkages in the SOM analysis.

Figure 5.1: Present observed adn modeled CCSM4 ice extent

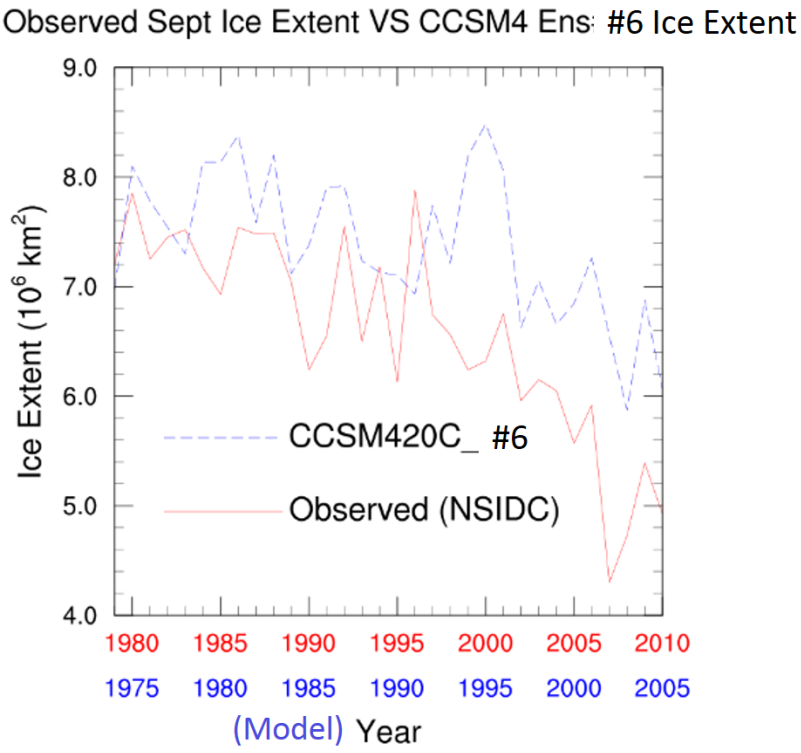

September observed sea ice extent (from NSIDC) (red line) for 1979 - 2010 and ensemble #6 from the CCSM4 20th century experiment ice extent for model year 1974 - 2005. Modeled sea ice extent is calculated using the area with sea ice concentrations of at least 15%.

Figure 5.2: ERA-Interim Mean JFM SLP

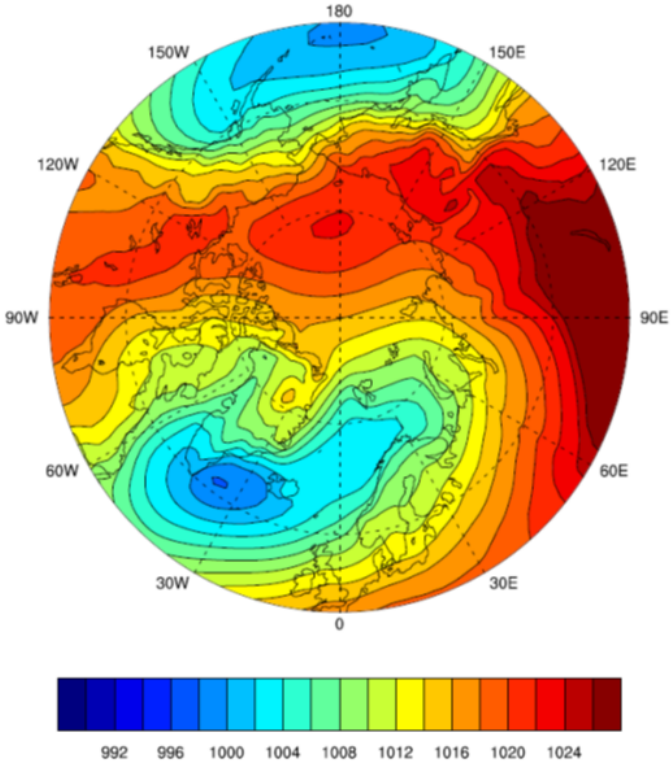

ERA-Interim seasonal mean JFM sea level pressure (mb) from 50-90 °N for the time period 1979-2010.

Figure 5.3: CCSM4 20th Century Mean JFM SLP

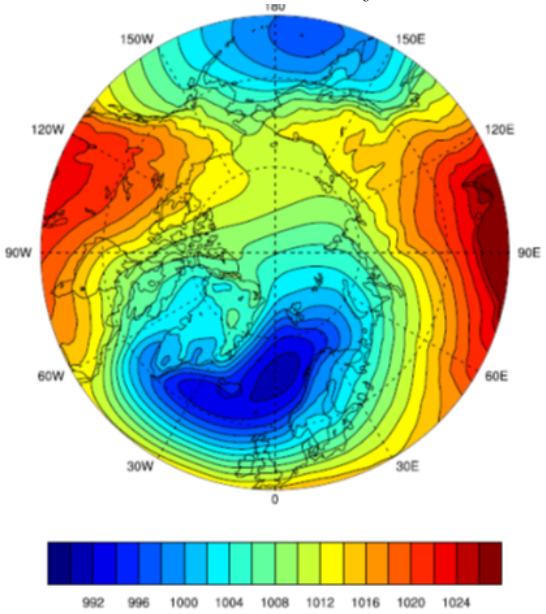

20th century (model year 1974-2005) mean winter JFM sea level pressure (mb) simulated by CCSM4 Ensemble #6 from 1979 - 2010 from 50-90 °N.

Figure 5.4: ERA-Interim Mean AMJ SLP

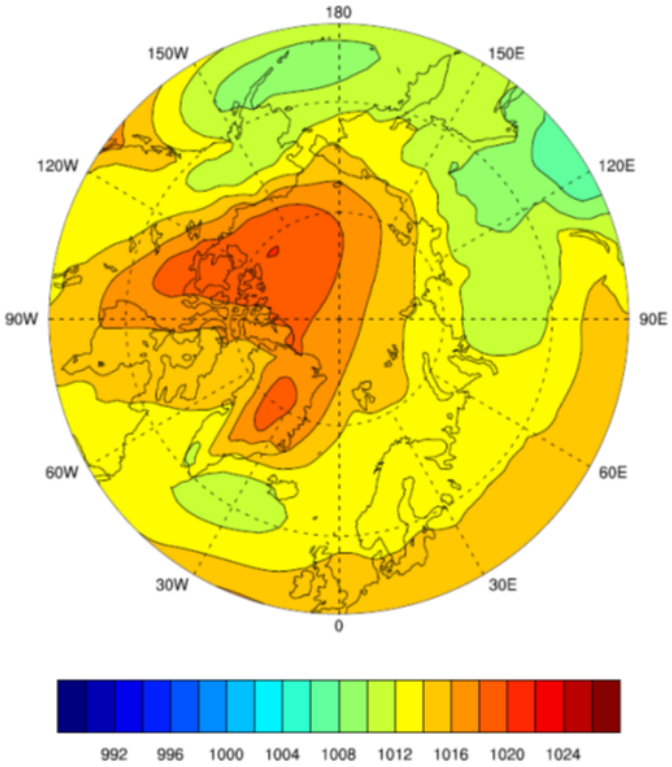

As in Figure 5.2, but for spring (AMJ).

Figure 5.5: CCSM4 20th Century Mean AMJ SLP

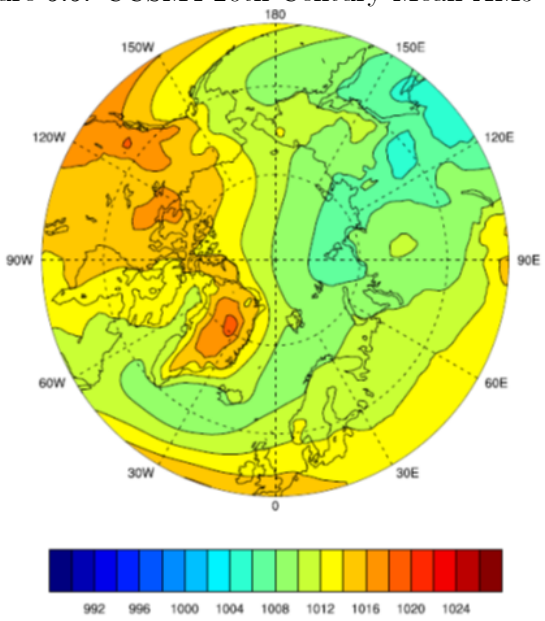

As in Figure 5.3, but for spring (AMJ).

Figure 5.6: ERA-Interim Mean April SLP

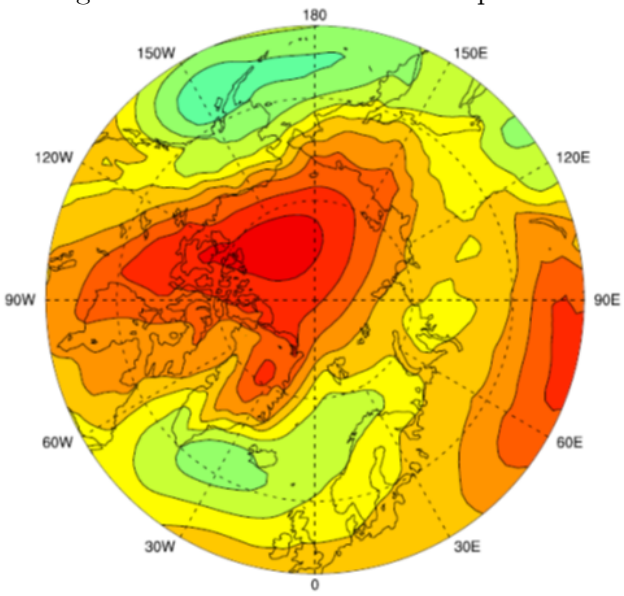

ERA-Interim mean April sea level pressure (mb) from 50-90 °N.

Figure 5.7: CCSM4 Mean April SLP

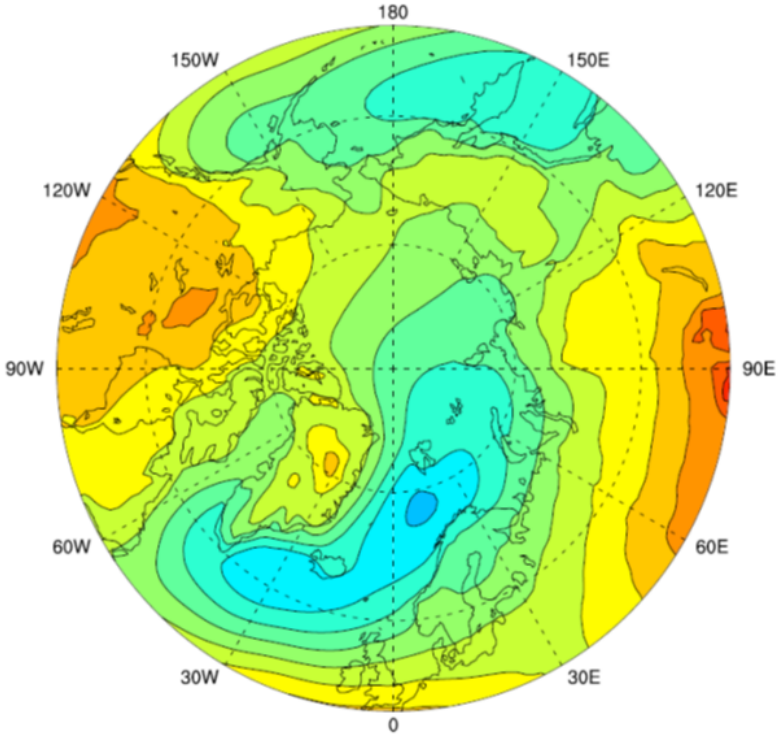

20th century (1974-2005) mean May sea level pressure (mb) as simulated by CCSM4 Ensemble #6 from 50-90 °N.

Figure 5.8: CCSM4 Mean May SLP

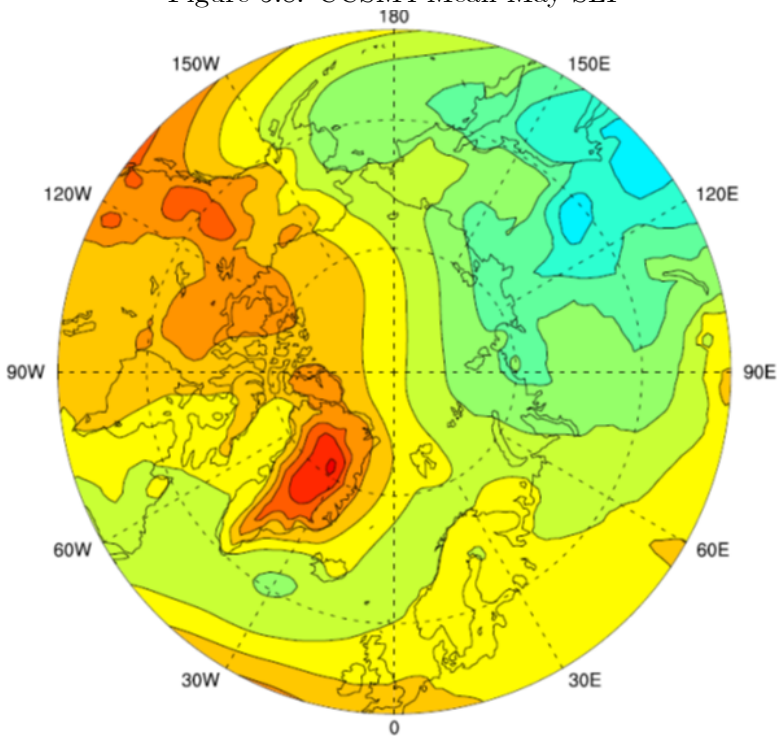

As in Figure 5.7, but for May.

Figure 5.9: ERA-Interim Mean JAS SLP

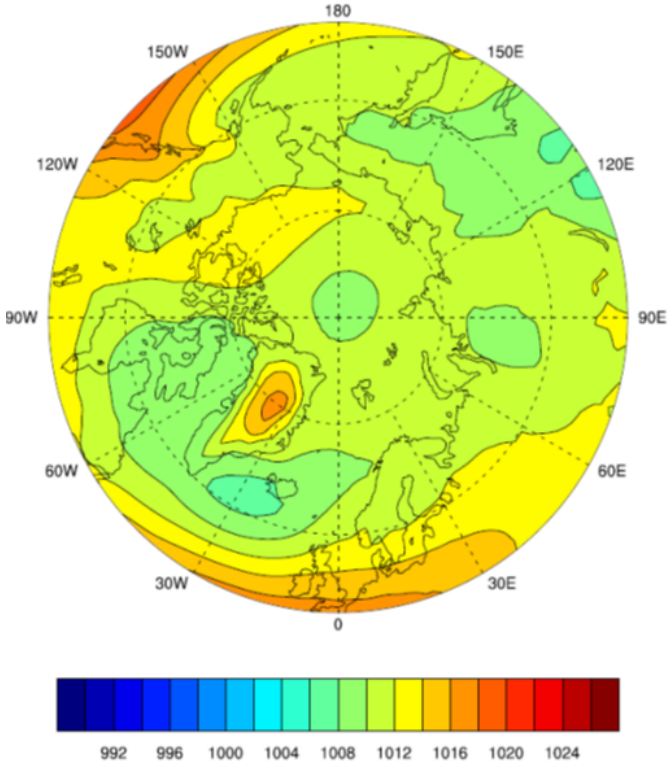

As in Figure 5.2, but for summer (JAS).

Figure 5.10: CCSM4 Mean JAS SLP

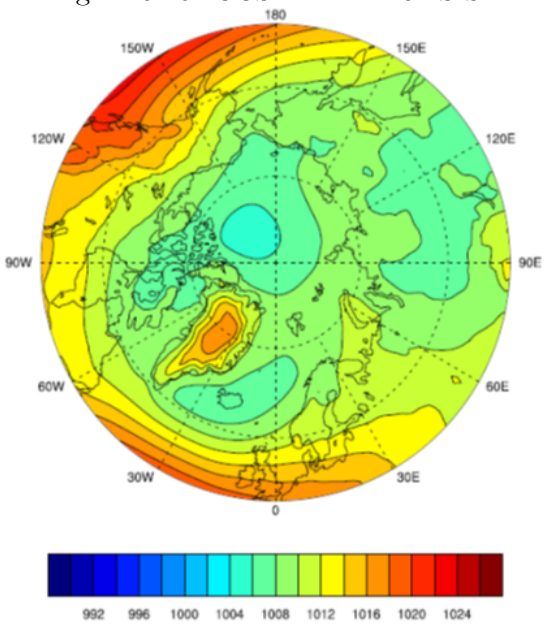

As in Figure 5.3, but for summer (JAS).

Figure 5.11: ERA-Interim Mean OND SLP

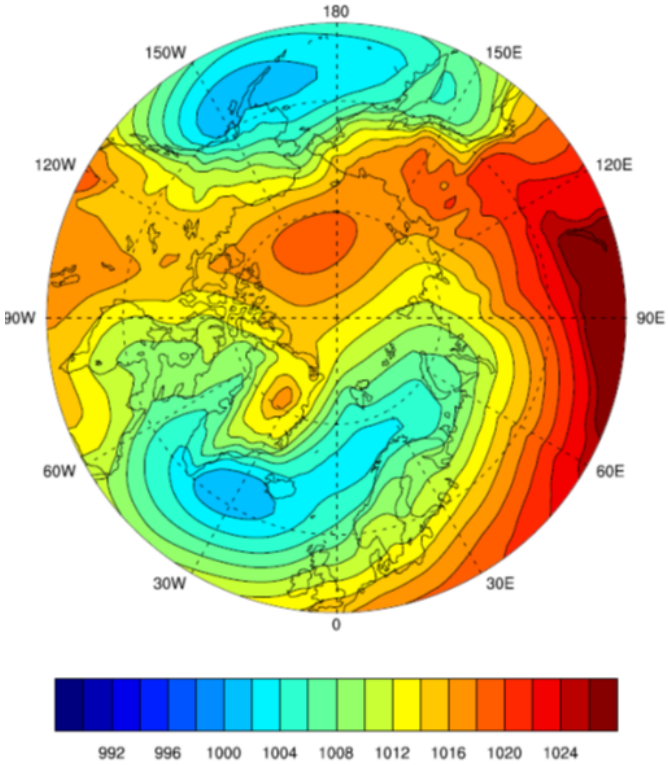

As in Figure 5.2, but for fall (OND).

Figure 5.12: CCSM4 Mean OND SLP

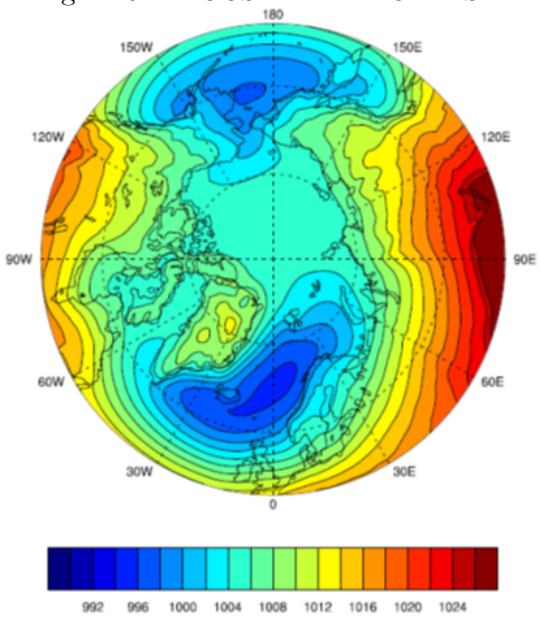

As in Figure 5.3, but for fall (OND).

Figure 5.13: Present observed and modeled CCSM4 ice extent

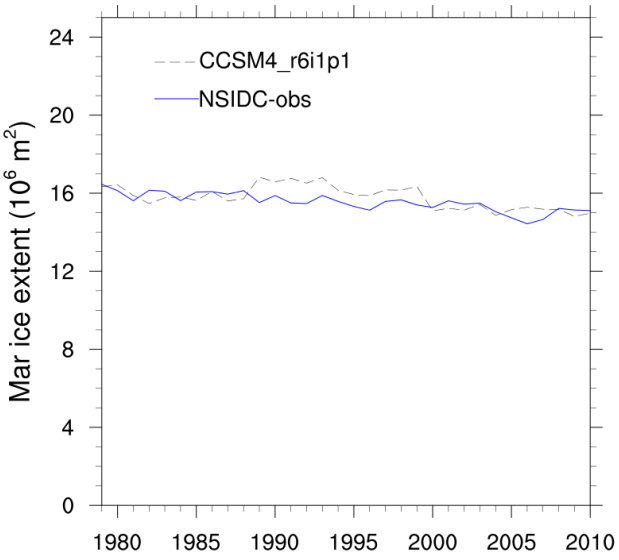

As in Figure 5.1, but for March.

Figure 5.14: ERAI and CCSM4 High Pressure Bridges group frequencies

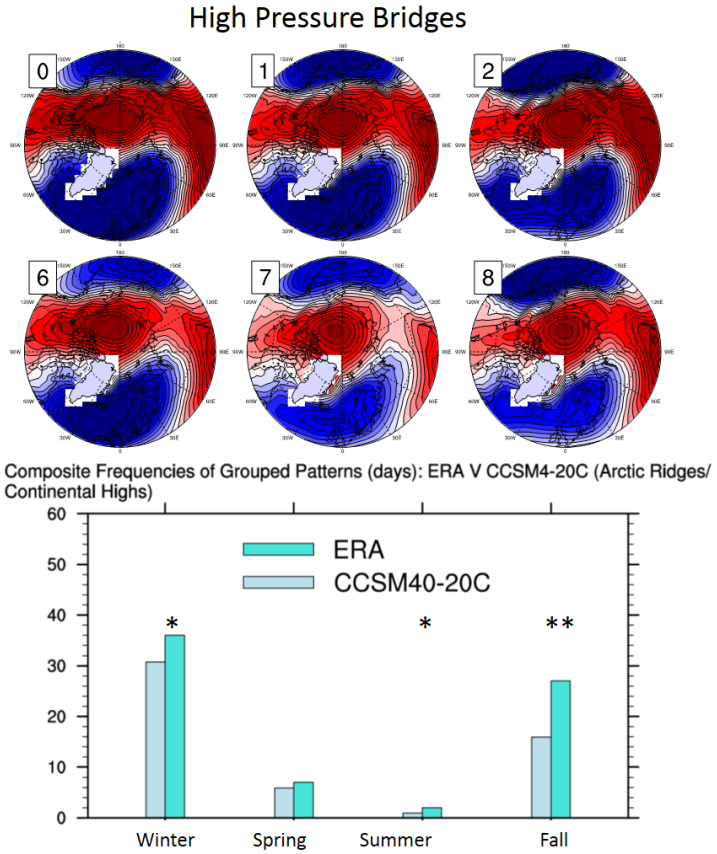

ERAI and CCSM4 High Pressure Bridges group frequencies mapped to ERAI Master SOM. One (**,***) asterisk(s) represents a statistically significant differences of at least 90% (95% and 99%, respectively).

Figure 5.15: ERAI and CCSM4 Eurasian Highs-Icelandic/Aleutian Lows group frequencies

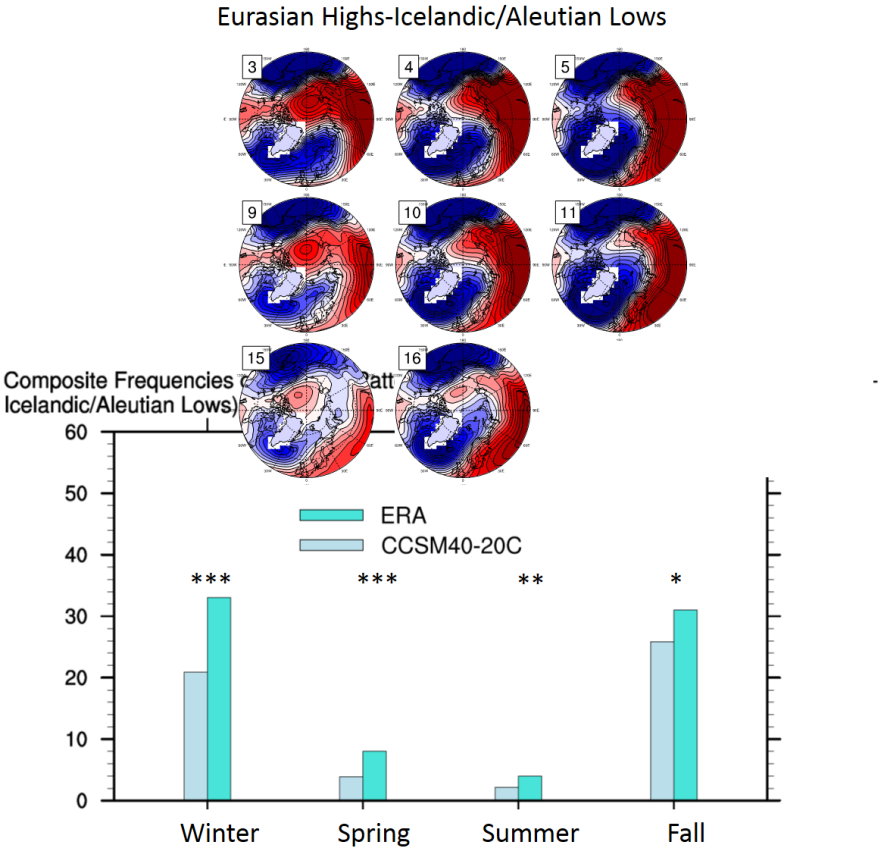

As in Figure 5.14, but for the Eurasian Highs-Icelandic/Aleutian Lows group.

Figure 5.16: ERAI and CCSM4 Arctic Highs/Pacific Lows group frequencies

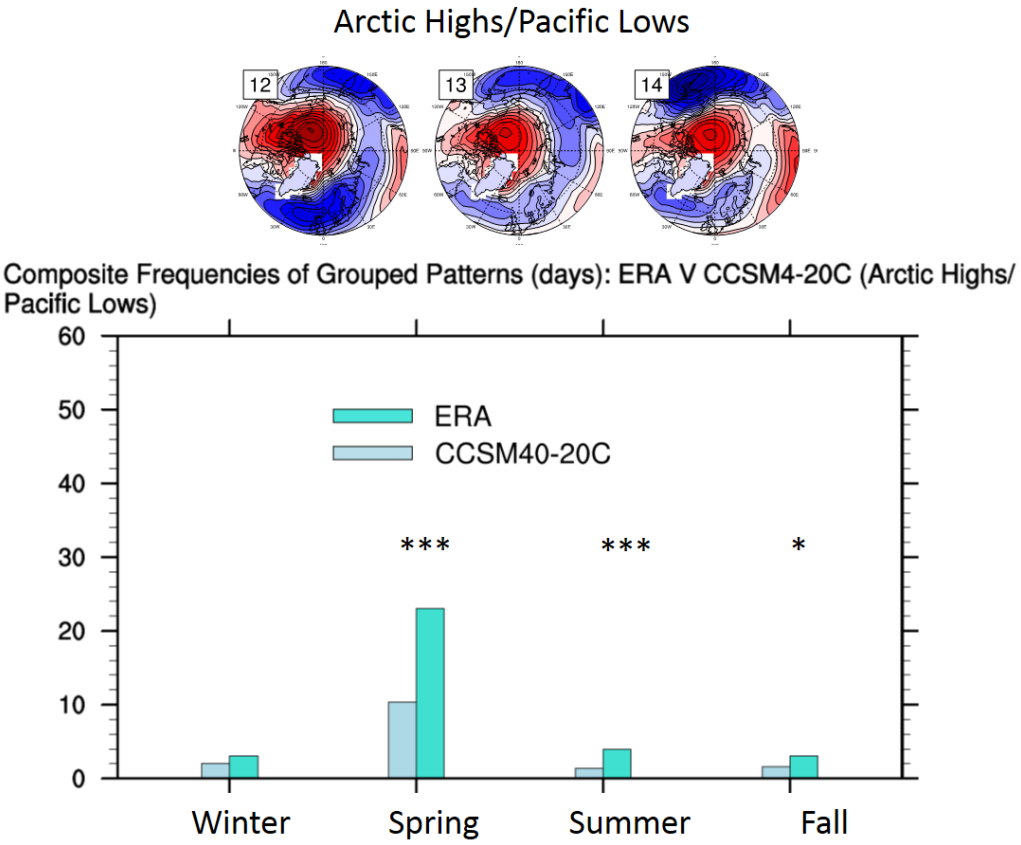

As in Figure 5.14, but for the Arctic Highs/Pacific Lows group.

Figure 5.17: ERAI and CCSM4 Icelandic Lows/Fram Strait Outflow group frequencies

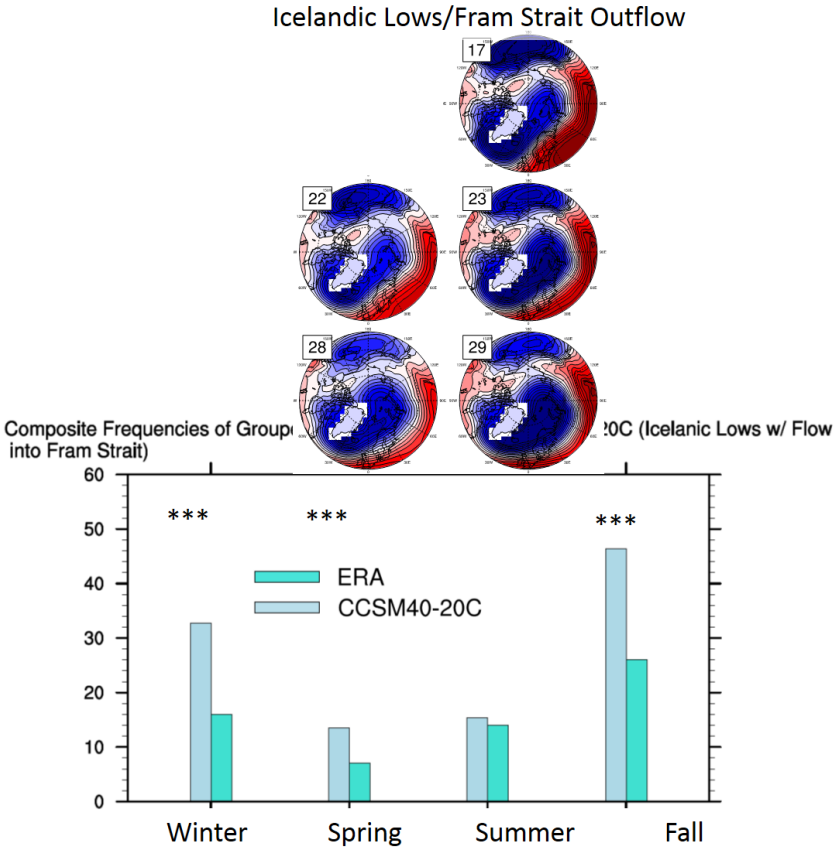

As in Figure 5.14, but for the Icelandic Lows/Fram Strait Outflow group.

Figure 5.18: ERAI and CCSM4 Beaufort Highs/Eurasian Lows group frequencies

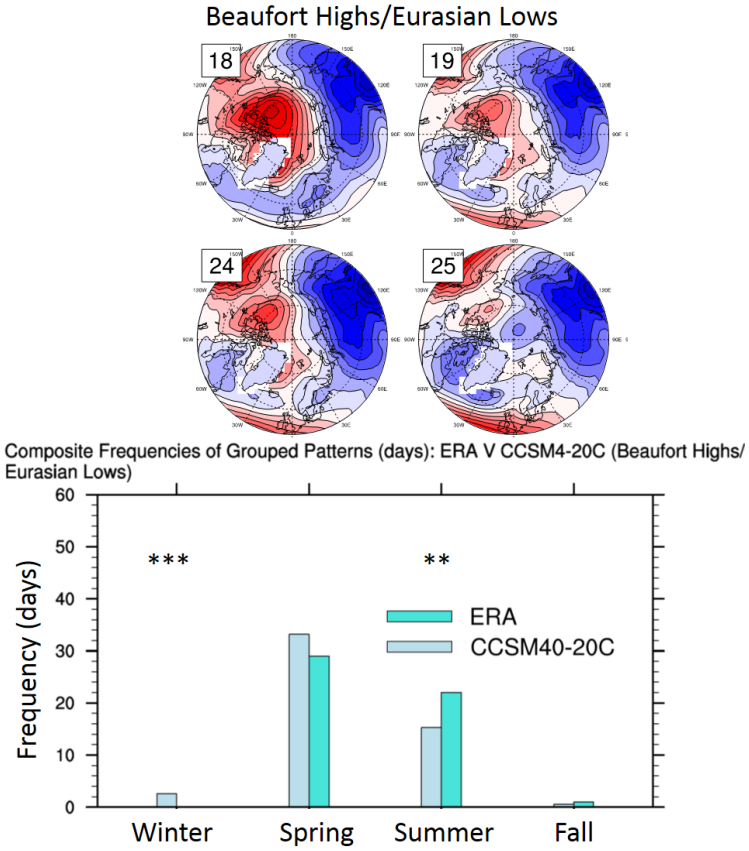

As in Figure 5.14, but for the Beaufort Highs/Eurasian Lows group.

Figure 5.19: ERAI and CCSM4 Weak Features group frequencies

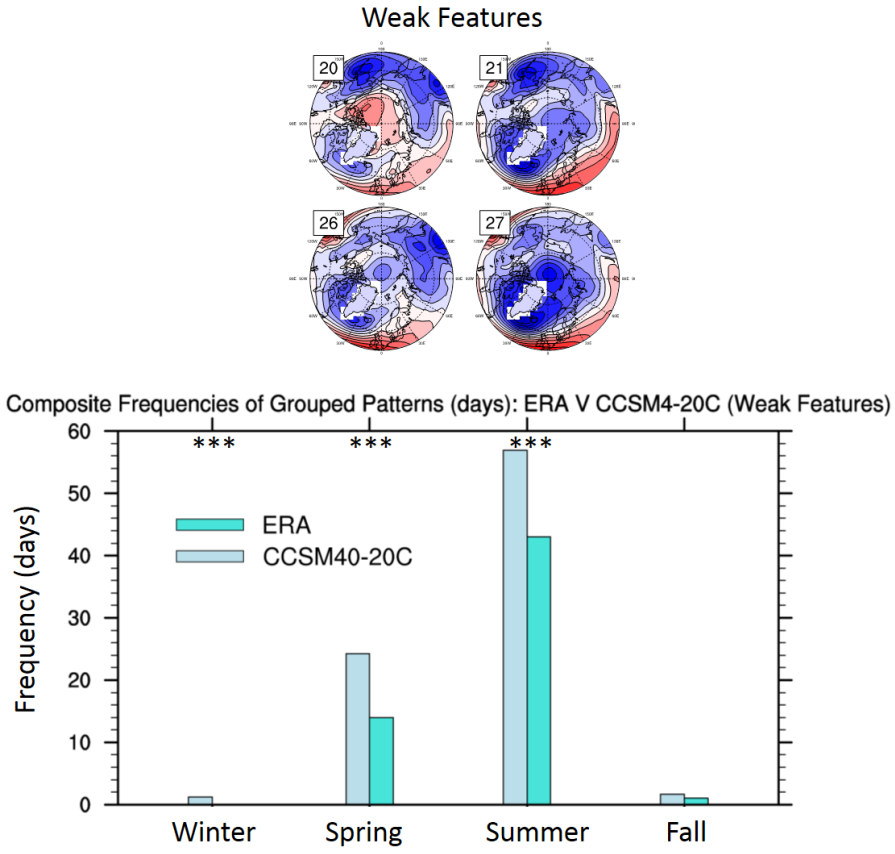

As in Figure 5.14, but for the Weak Features group.

Table 5.1: Correlations b/w CCSM4 Ens 6 frequencies from ERAI Master SOM and modeled year-to-year change in Sep ice exent

	JFM	**AMJ**	**JAS**	**OND (yr N-1)**
High Pressure Bridge	0.01	-0.07	0.18	**-0.34***
Eurasian H-Ice/Al Lows	-0.07	-0.13	-0.07	-0.1
Arctic Highs/Pac Lows	0.08	-0.2	0	-0.08
Ice L/FS Outflow	**-0.34***	-0.19	-0.29	**0.32***
Beaufort H/Eura Lows	-0.09	-0.08	0.14	-0.12
Weak Features	-0.06	-0.25	0	-0.01

Correlations between CCSM4 20th century Ensemble #6 frequencies (mapped to the ERAI Master SOM in Figure 3.2) and year-to-year change in September ice extent (from 1975-2005) simulated by CCSM4 20th century Ensemble #6. One asterisk indicates statistical significance at 90% or greater.

Figure 5.20: ERAI and CCSM4 Bias-Corrected High Pressure Bridges group frequencies

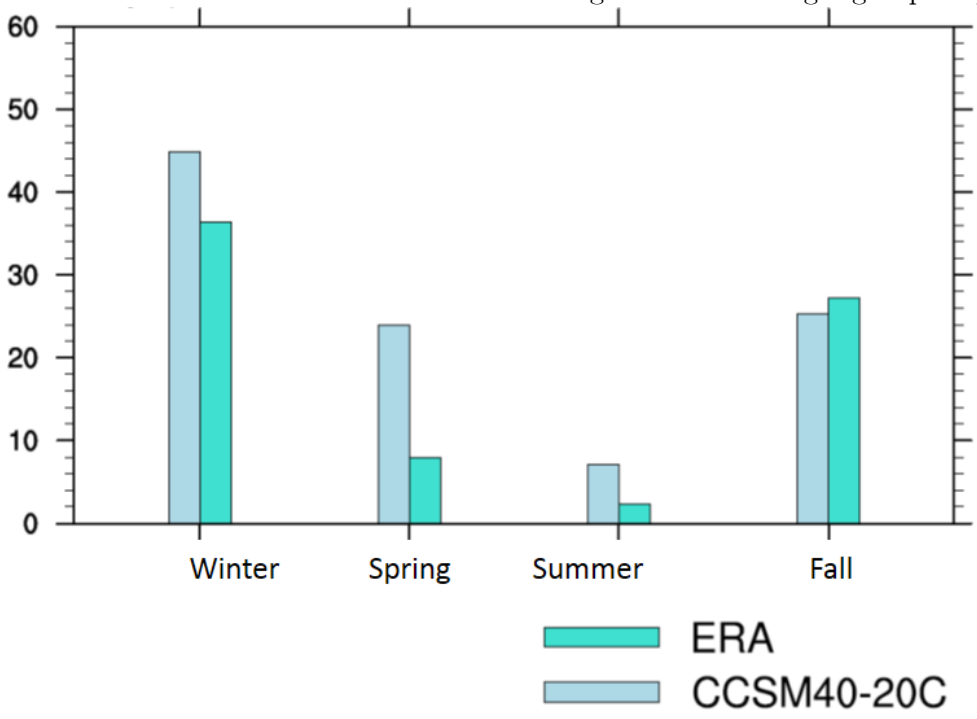

As in Figure 5.14, but for the bias-corrected CCSM4 SLP daily fields, discussed in the text (and statistical significances and SOM group SLP fields are not shown).

Figure 5.21: ERAI and CCSM4 Bias-Corrected Beaufort Highs/Eurasian Lows group frequencies

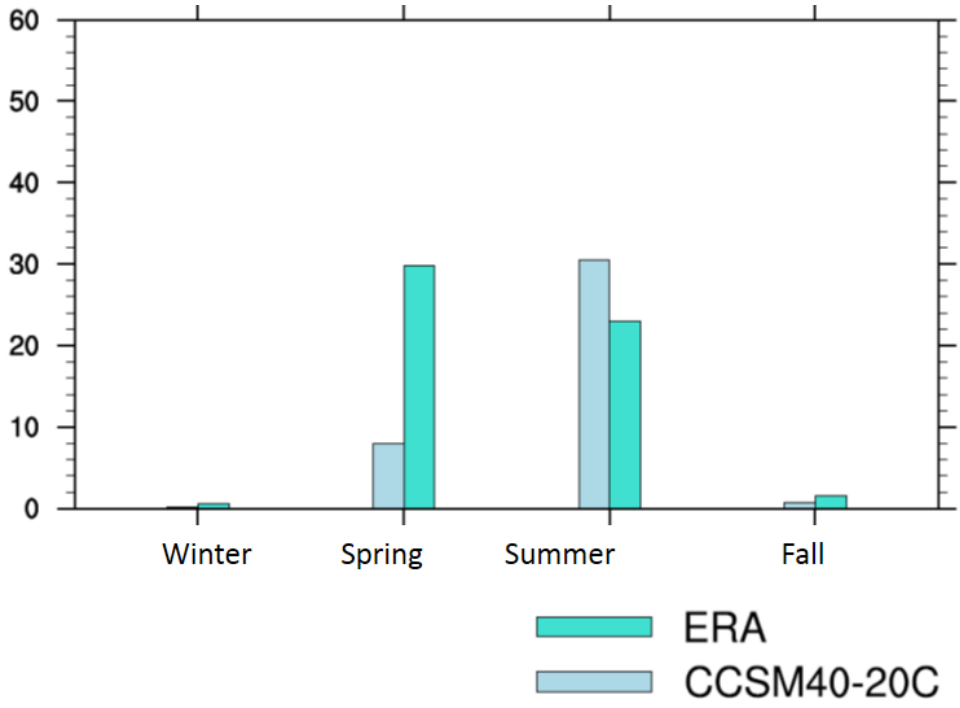

As in Figure 5.20, but for the Beaufort Highs/Eurasian Lows group.

Figure 5.22: ERAI and CCSM4 Bias-Corrected Weak Features group frequencies

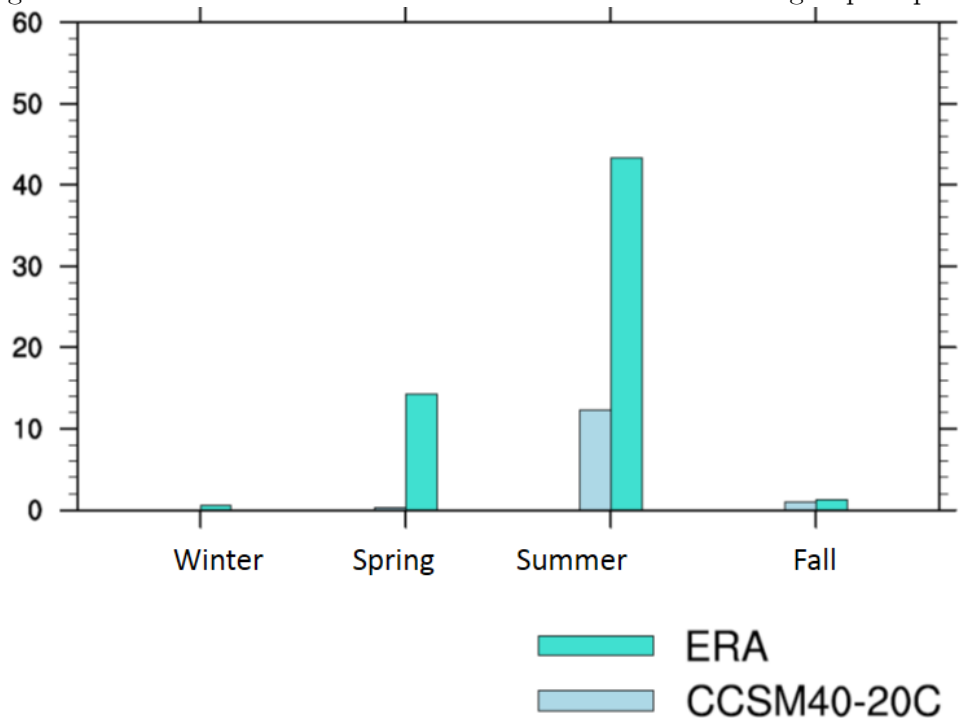

As in Figure 5.20, but for the Weak Features group.

Figure 5.23: ERA Downwelling LW radiation: High Pressure Bridges

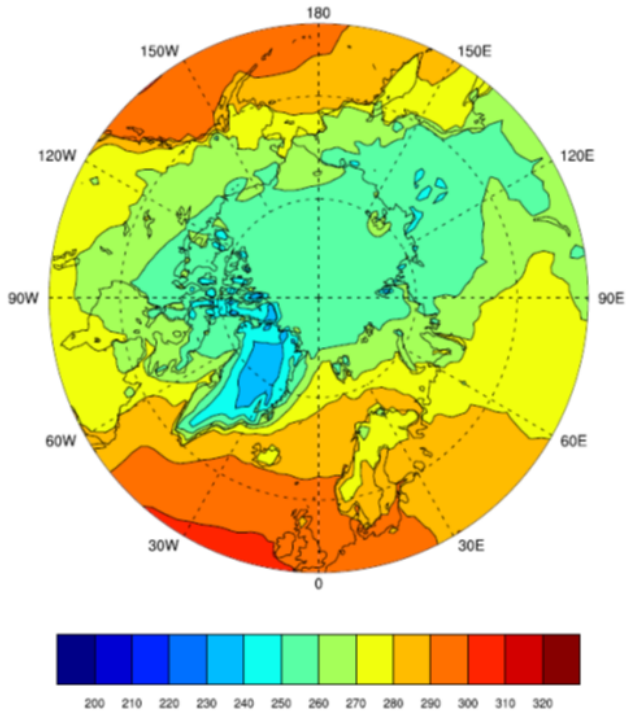

Mean downwelling longwave radiation field for the "High Pressure Bridge" group in the ERA Interim Master SOM, shown in Figure 3.2. The field was computed by averaging daily downwelling longwave radiation fields for the days that mapped to patterns within the "High Pressure Bridge" group as the best matching unit (BMU).

Figure 5.24: CCSM4 Downwelling LW radiation: High Pressure Bridges

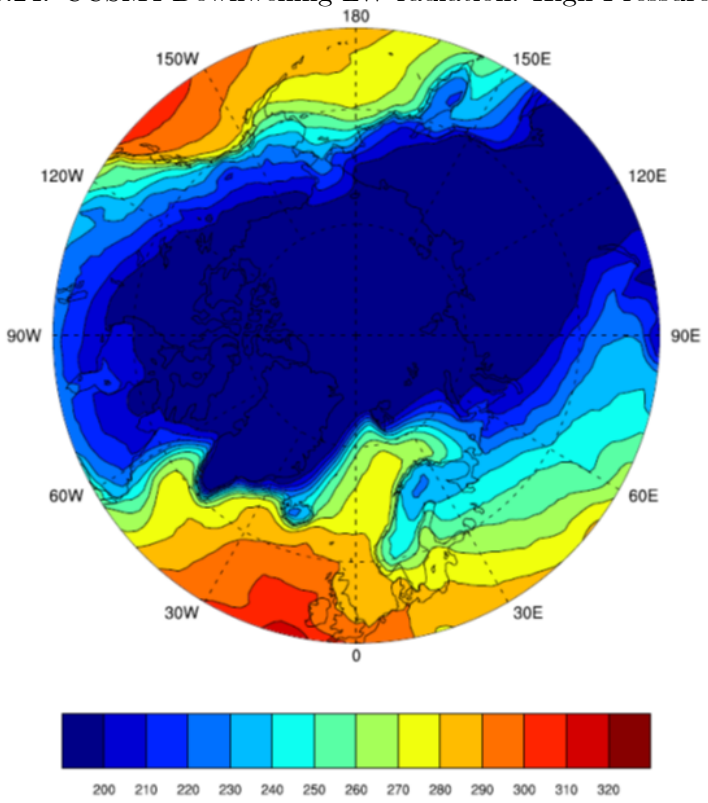

As in Figure 5.23 but for CCSM4.

Figure 5.25: ERA Arctic Oscillation SLP patterns

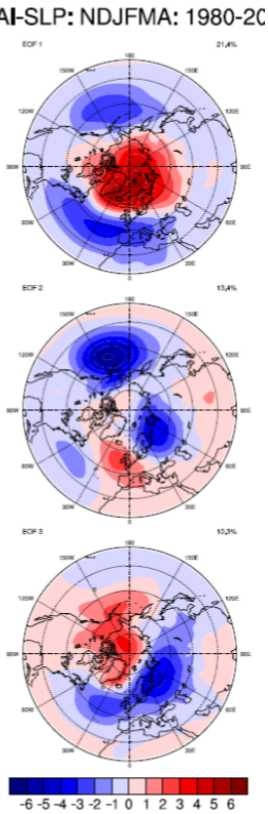

Spatial patterns of extended winter NDJFMA monthly mean SLP anomalies regressed onto the standardized time series of the three leading principal component analysis of SLP from 20-90 °N. The AO is defined as the leading PC.

Figure 5.26: ERA Arctic Oscillation standardized time series

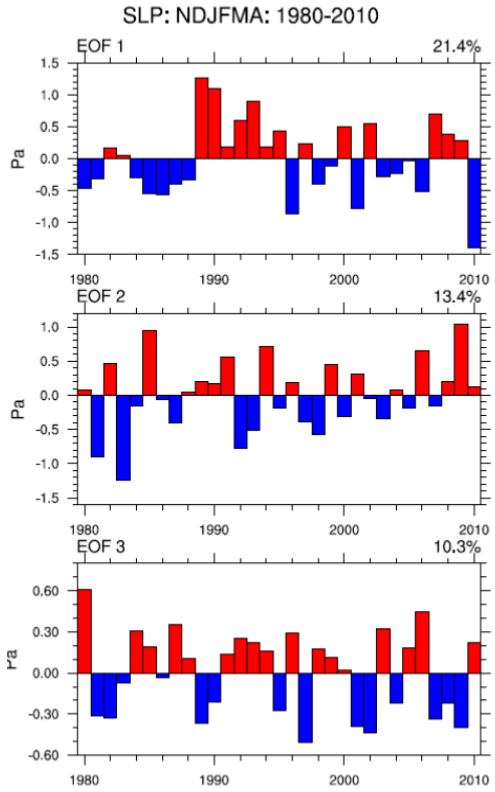

Regression coefficients from three leading principal components of extended winter ND-JFMA monthly mean SLP anomalies from 20-90 °N. The AO is defined as the leading PC.

Figure 5.27: CCSM4 Arctic Oscillation SLP patterns

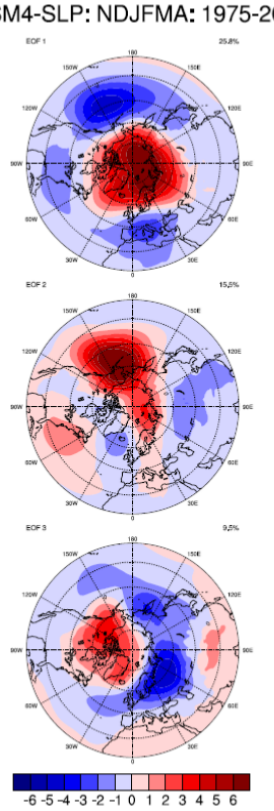

As in Figure 5.25 but for CCSM4.

Figure 5.28: CCSM4 Arctic Oscillation standardized time series

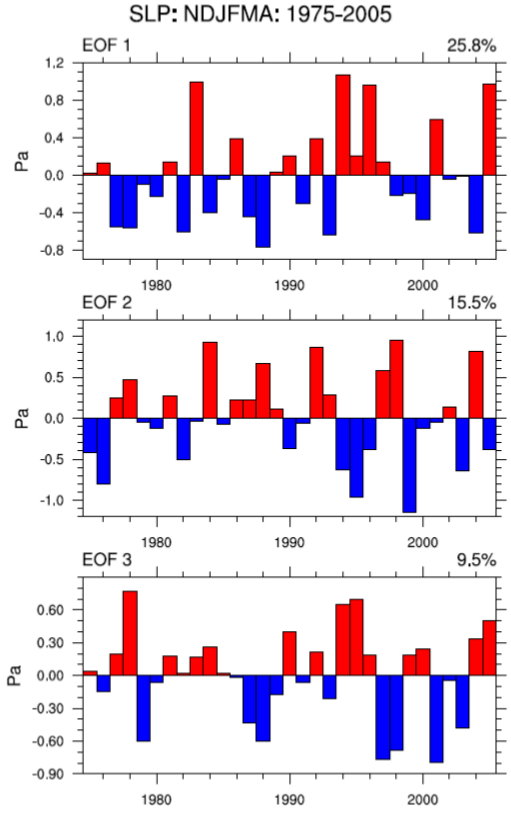

As in Figure 5.26 but for CCSM4.

Figure 5.29: ERA North Atlantic Oscillation SLP patterns

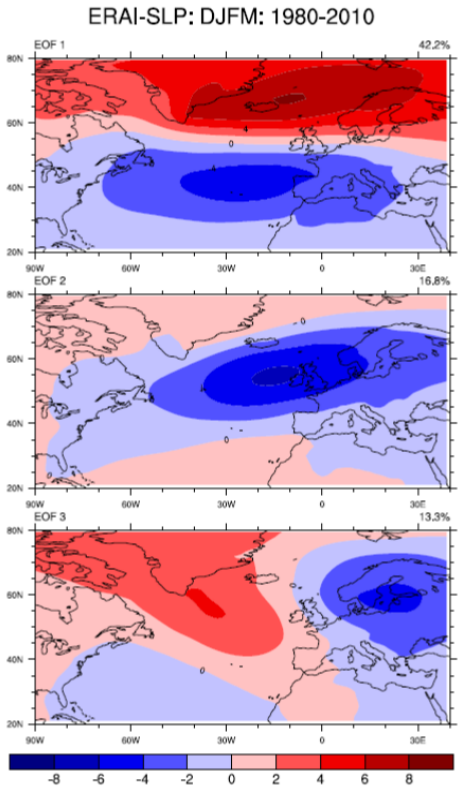

Spatial patterns of extended winter DJFM monthly mean SLP anomalies regressed onto the standardized time series of the three leading principal component analysis of SLP from 20-90 °N and 90°W-40 °E. The NAO is defined as the leading PC.

Figure 5.30: CCSM4 North Atlantic Oscillation SLP patterns

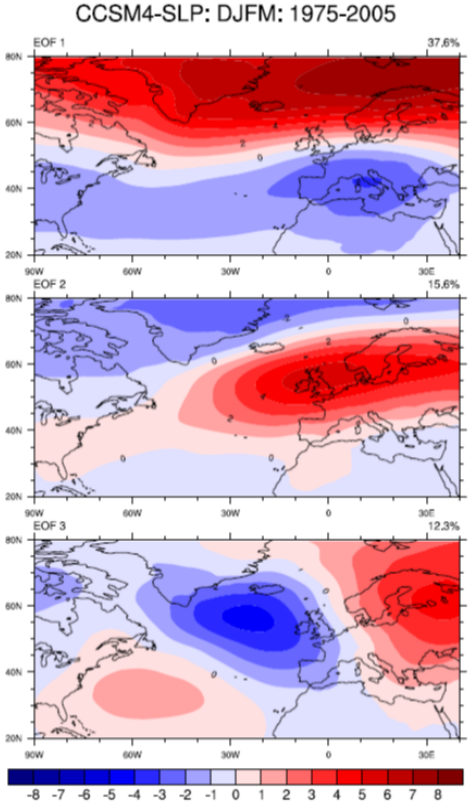

As in Figure 5.29 but for CCSM4.

Figure 5.31: ERA North Atlantic Oscillation standardized time series

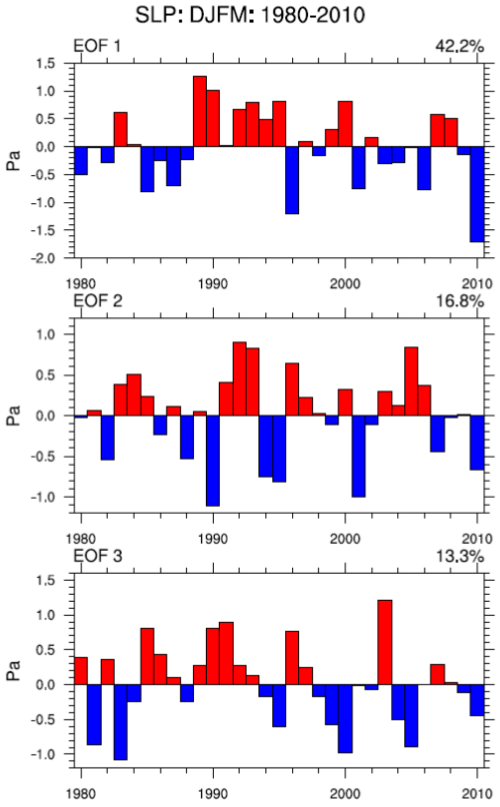

As in Figure 5.26 but for the NAO.

Figure 5.32: CCSM4 North Atlantic Oscillation standardized time series

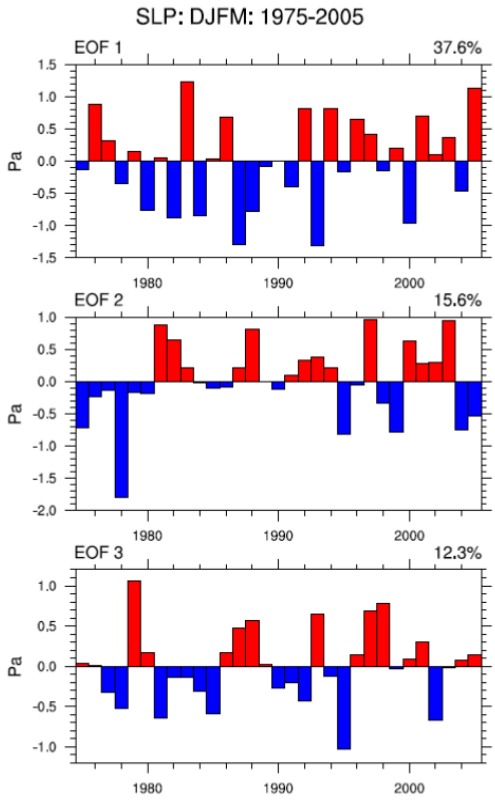

As in Figure 5.31 but for CCSM4.

Figure 5.33: ERA Arctic Dipole SLP patterns

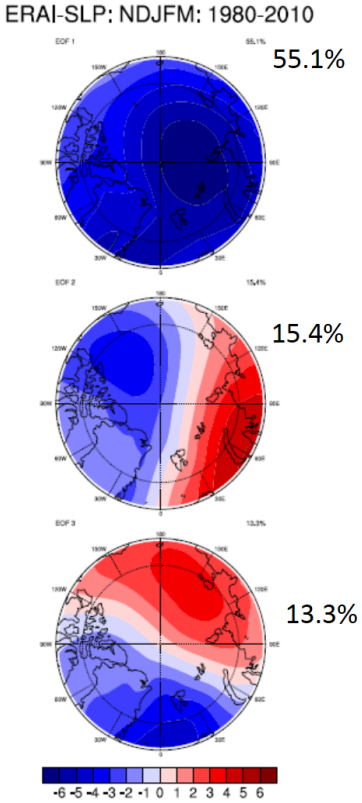

Spatial patterns of extended winter DJFM monthly mean SLP anomalies regressed onto the standardized time series of the three leading principal component analysis of SLP from 70-90 °N. The Arctic Dipole is defined as the second leading PC. The first resembles the AO.

Figure 5.34: CCSM4 Arctic Dipole SLP patterns

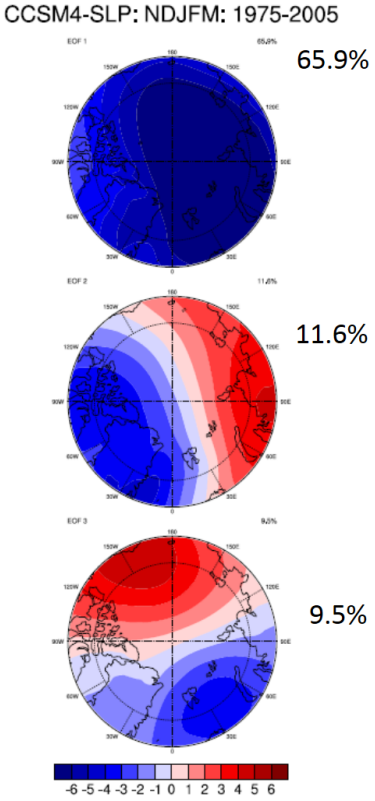

As in Figure 5.33 but for CCSM4.

Figure 5.35: ERA Arctic Dipole standardized time series

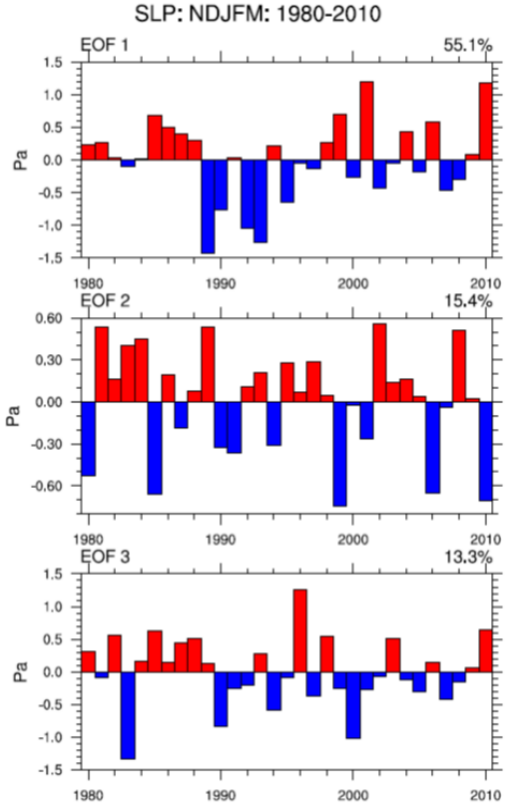

As in Figure 5.26 but for the AD.

Figure 5.36: CCSM4 Arctic Dipole standardized time series

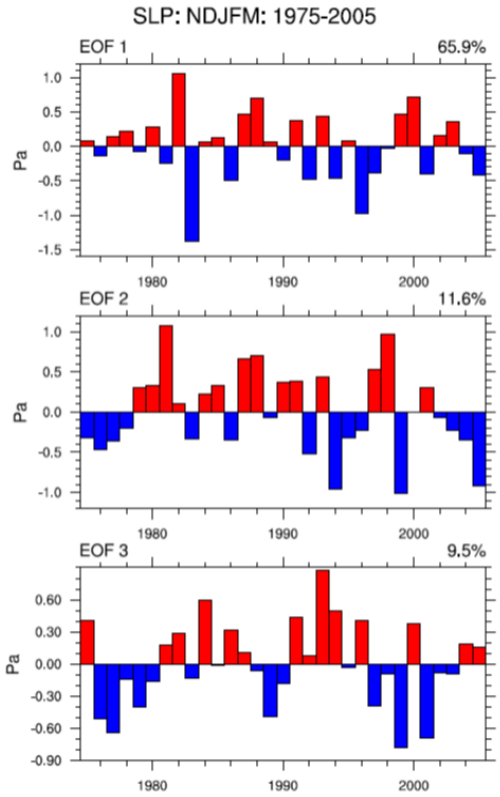

As in Figure 5.35 but for CCSM4.

Table 5.2: CCSM4 Teleconnection Indices Correlated to delSIE

	Teleconnection Pattern		
	AO	NAO	AD
Winter	-0.22	0.26	-0.02
Spring	-0.13	-0.05	0.55***
Summer	-0.12	0.07	0.18
Fall (yr N-1)	-0.16	0.01	0.18

Correlations between seasonal (JFM, AMJ, JAS of year N, and OND of year N-1) teleconnection patterns (AO, NAO, and AD), defined in the text, within CCSM4 20th century Ensemble #6 and year-to-year change in September ice extent (from 1975-2005) simulated by CCSM4 20th century Ensemble #6. One asterisk (**, ***) indicates statistical significance at 90% (95%, 99%) or greater.

Figure 5.37: Ice Motion associated with AO: Obs and Model

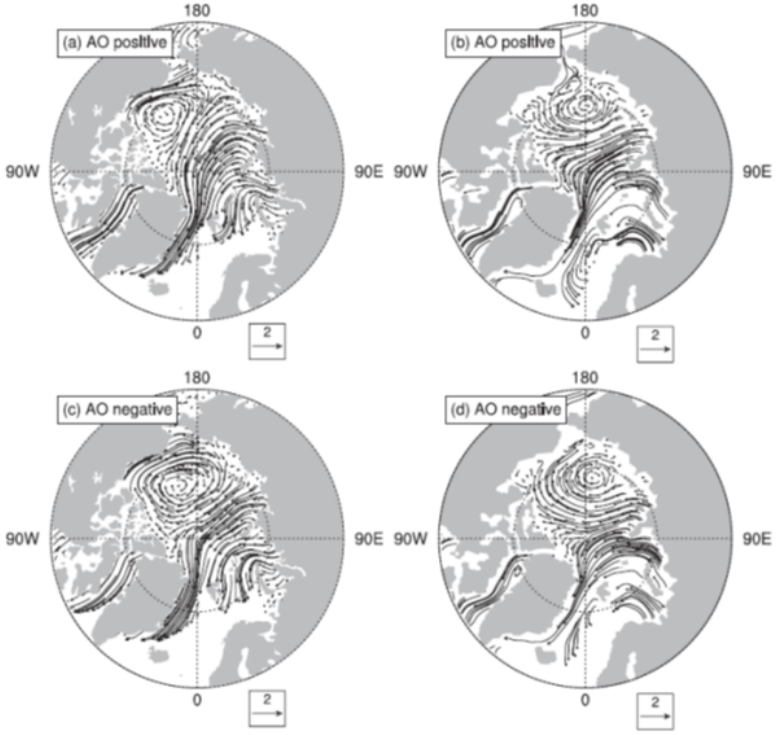

Mean DJFM ice motion fields for years associated with the positive AO years (top) and negative AO years (bottom) from satellite observations (left) and CCSM4 present-day climate (right). Taken from Jahn et al. (2011), Figure 9.

Figure 5.38: CCSM4 20th Century Mean JFM SLP Ens 4

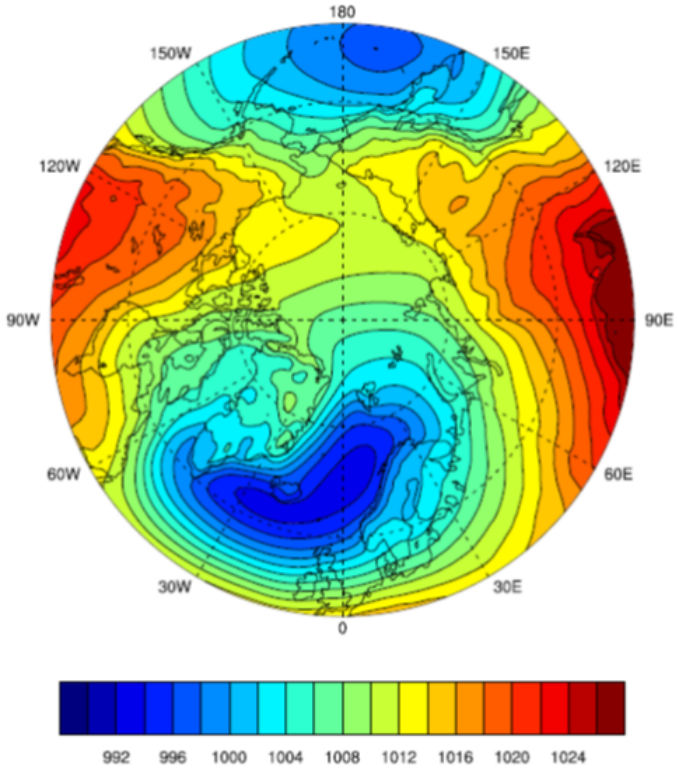

As in Figure 5.3, but for JFM for Ensemble 4.

Figure 5.39: CCSM4 20th Century Mean JFM SLP Ens 5

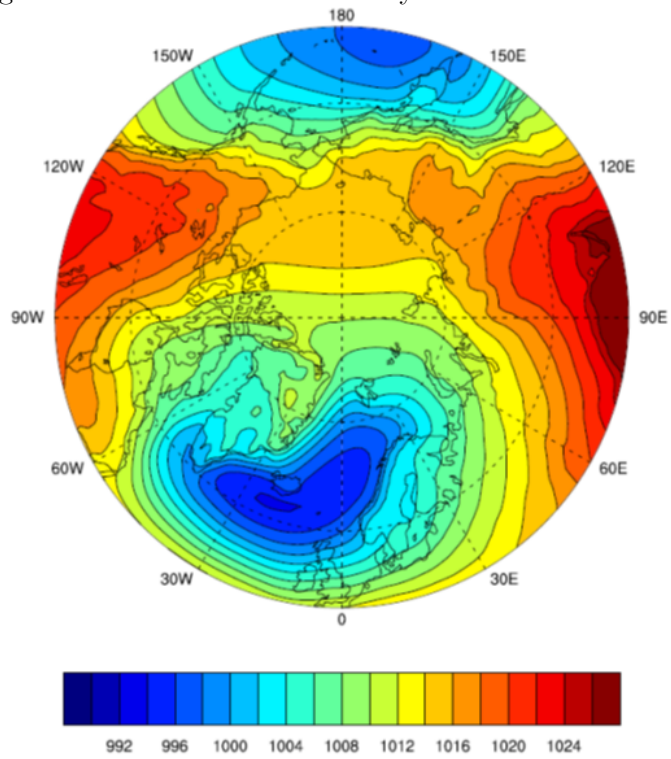

As in Figure 5.3, but for JFM for Ensemble 5.

Figure 5.40: CCSM4 20th Century Mean AMJ SLP Ens 5

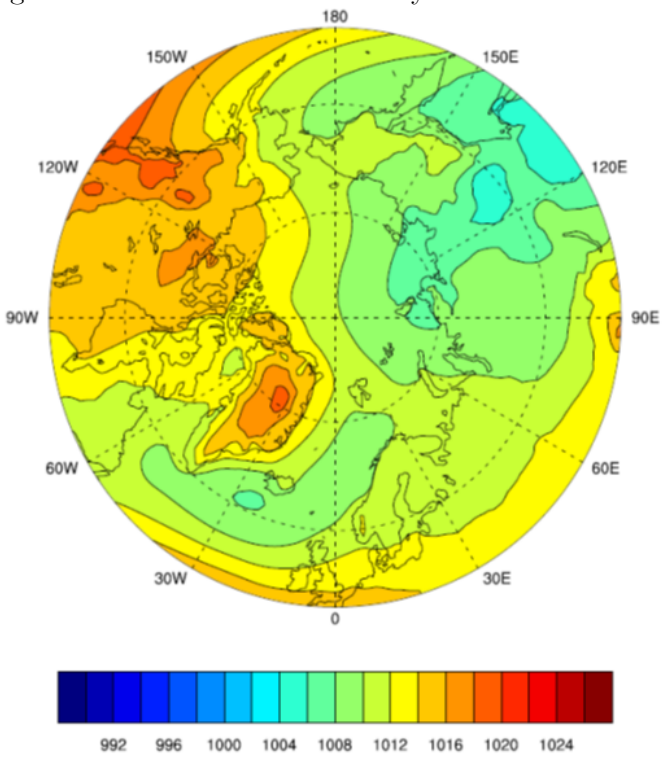

As in Figure 5.3, but for AMJ for Ensemble 5.

Figure 5.41: CCSM4 20th Century Mean JAS SLP Ens 4

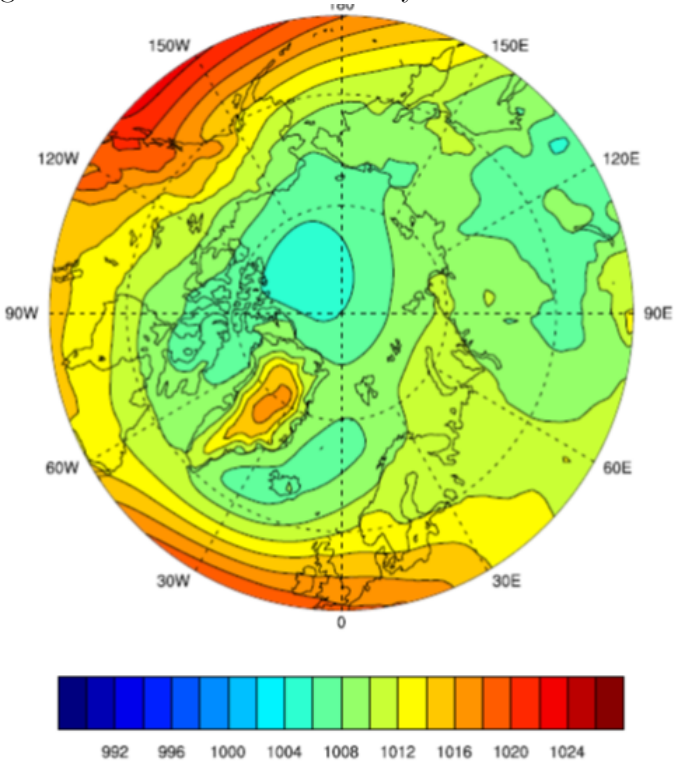

As in Figure 5.3, but for JAS for Ensemble 4.

Figure 5.42: CCSM4 20th Century Mean JAS SLP Ens 5

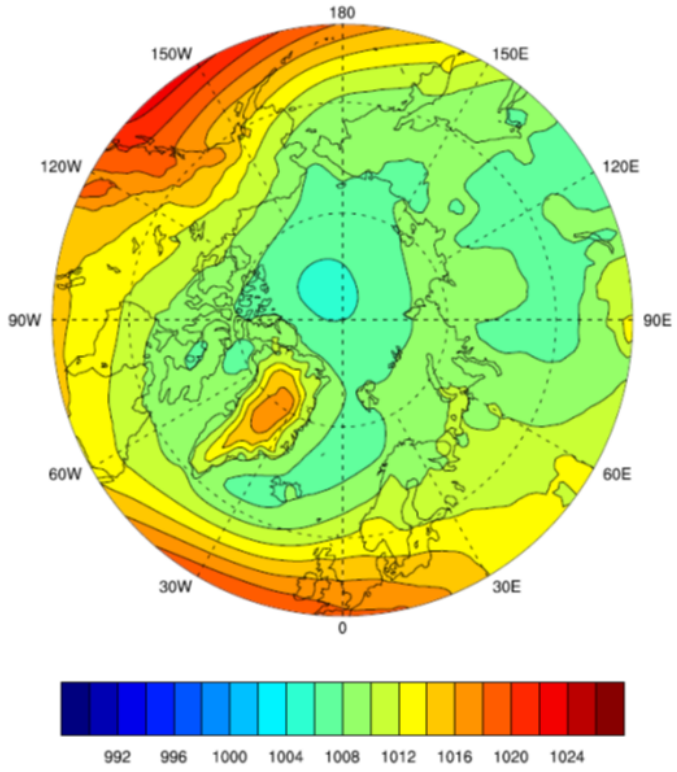

As in Figure 5.3, but for JAS for Ensemble 5.

5.2 Synoptic Activity in CCSM4: Present-Day Climate Vs. Future Climate

The CCSM4 present-day and 21st century climates were used to train a 6x5 master SOM. Model years 1974 to 2005 and 2069 to 2100 are used from each respective experiment so that the length of comparison periods are identical. This method was chosen over simply comparing the 21st century climate to ERA-Interim as was done in the previous section since the present-day climate had issues simulating the observed patterns and capturing the associated ice variability linkages, suggesting that the CCSM4 synoptic activity has a different representations of day-to-day SLP not captured by the ERA-Interim Master SOM.

The CCSM4 Master SOM is shown in Figure 5.43. The patterns were grouped analogously to the ERAI Master SOM grouping discussed in Chapter 3. Groupings were objectively categorized based on spatial correlations and similar spatial patterns. The SOM features the main Arctic circulation patterns (Serreze and Barry (2005)). Broad Arctic High pressure ridges that span the ice cover and subpolar continents that dominate in winter (Figure 5.44) are featured in the top-left portion of the SOM. Strong storm tracks that predominate in fall and winter, but can occur in all seasons, are featured on the right-side. Weaker pressure features associated with weakening Arctic circulation during the warm season are featured on the bottom-left. The CCSM4 Master SOM also appears similar to the ERA-Interim Master SOM. Some apparent differences are the more predominant low pressures over the central Arctic in CCSM4 (the right portion of Figure 5.43) and fewer broad high pressure patterns over the ice (similar to those in the top portion of the ERA-Interim Master SOM, shown in Figure 3.2). This is due to 1) CCSM4's low pressure bias (see the previous section) and 2) SLP

over the Arctic deepening in the 21st century CCSM4 climate (Vavrus et al. (2011)). Figure 5.44 displays the mean seasonal frequencies for each group from Figure 5.43 for both the 20th and 21st centuries. Like the ERA-Interim Master SOM (Figure 3.2), the patterns display prominent seasonality.

Table 5.3 shows the 20th century CCSM4 mean annual grouped frequencies for each season when mapped to the CCSM4 Master SOM (Figure 5.43). During winter, Group 1 in Figure 5.43 predominates, occurring on average ~37 days out of the 90 day season, with broad high pressures over the ice cover and continents. Group 1 is quite similar to the "High Pressure Bridges" group in Figure 3.2 (the ERA-Interim Master SOM), although the CCSM4 Master SOM does not produce as many high pressure weather patterns. The high pressure patterns that are simulated generally do not have pressure gradients conducive to flow through the Fram Strait that was earlier shown to be important for year-to-year ice loss (e.g., patterns 1 and 7 in Figure 5.43, which have pressure gradients that are conducive to packing ice on the northern side of Greenland). Winds associated with high pressure features have been shown to be important to recent record ice losses (Ogi et al. (2010)). Group 4 is the next most prominent winter group (mean frequency of 25 days per season), which features the Icelandic and Aleutian low storm tracks and strong low pressure features over the ice cover, which are not present in the observations during winter (Figure 3.2 and see Serreze and Barry (2005)). Consistent with de Boer et al. (2011), Group 4 displays storm tracks that penetrate too far northward into the Arctic, especially during winter. Screen et al. (2011) showed that an increase in cyclonic activity over the central Arctic during MJJ helped to preserve ice cover in the subsequent September. It is unclear, however, if this would be the case during winter, as the effect of synoptic activity or storms on winter ice variability has not been extensively studied to my

knowledge. Group 2, similar to the "Beaufort Highs/Eurasian Lows" group in Figure 3.2, are also a predominantly spring group (occurring ~23 days annually). Group 3 is most similar to the "Weak Features" group in the ERAI Master SOM and is also a predominantly summer group (occurring ~17 days annually), but low pressures are deeper.

During spring, Group 2, dominated by high pressures, occurs ~32 days on average. The next most prominent spring group is Group 5, occurring 20 days on average. The model simulates strong high pressure bridges ~15 days during the spring season (Group 0). During summer, Groups 3 and 5 occur 75% of the summer season (mean frequency of occurrences of approximately 17 and 51 days, respectively), associated with the summer cyclone maximum over the ice. This further signals the model's failure in simulating Beaufort Highs during the summer associated with ice loss (e.g., Chapter 4 and de Boer et al. (2011)). Fall resembles winter with Group 0 occurring 18 days our of the season, although stronger-than-observed low pressure signals still dominate, with Groups 1 and 4 occurring ~34 and 33 days on average during the season, respectively.

An important aspect to investigate is the change in synoptic activity between the 20th and 21st centuries as the Arctic climate is projected to prominently change. Maslanik et al. (2011) discussed the increased mobility of a thinner ice pack, so quantifying projected changes in synoptic activity is relevant to many issues, such as inundation and erosion of coastal Arctic communities and associated with enhanced wave activity from cyclones in an increasingly ice free Arctic and vessel navigation for naval and private prospects. Arctic ice extent is projected to become ice free (ice extent spanning less than one million km^2) in September by 2074 in Ensemble #6 (Figure 5.45).

Table 5.4 shows the mean annual frequencies by season for the CCSM4 21st daily SLP

fields mapped to the CCSM4 Master SOM (Figure 5.43). Composite differences for each season (21st century minus 20th century) are displayed in Figure 5.46. The most prominent differences occur in summer (JAS), likely associated with an essentially ice free Arctic during September (with pan-Arctic ice extent less than one million km^2). This finding contrasts to Vavrus et al. (2011), who showed that autumn (specifically November, followed by October) were the months during which the most drastic Arctic climate change occurred for all variables investigated (e.g., SLP, air temperature, and ice concentration). This could also be associated with temporal resolution, as Vavrus et al. (2011) studied the full 21st century run (2006 to 2100). This is associated with SOM group mean SLP fields decreasing in pressure in the 21st century climate (not shown). This, however, highlights SOM's utility as an additional too to study synoptic climatology in a changing climate. Features that may be averaged out of seasonal composites are captured in the full synoptic setup portrayed by SOMs.

Figure 5.46 shows a sharp increase in strong low pressure patterns (Group 5) by ~12 days annually (statistically significant at 90%) at the expense of all other patterns. For example, Groups 2 and 3, associated with weaker features, show a 90% statistically significant decrease of approximately 4 days. This finding is consistent with Cassano et al. (2006), which studied several CMIP3 ensembles and found an increase of strong low pressure patterns over the central Arctic and near Greenland during winter. Fall (OND) exhibits the next most prominent pattern changes, with a decrease in the Arctic high pressures in Group 0 high pressure patterns (by ~6 days, statistically significant at 90%). All other groups show an increase, up to ~5 days annually (Group 4), though not robust. Winter shows an increase in strong Arctic lows of Group 5, by nearly 2 days (statistically significant at 95%). The most prominent changes (although not robust at 90% statistical significance) are a decrease in strong North Atlantic

storm tracks (Group 4) by about 5 days annually during winter (not robust). An increase in Groups 4 and 5 highlights the projected northward shifting storm track in a changing climate as the temperature gradient shifts northward (Bengtsson et al. (2006)). The decrease in winter high pressures is consistent with Cassano et al. (2006). They also noted an increase in strong North Atlantic storms during winter. Group 1, with both strong Aleutian Lows and strong Icelandic Lows, shows an increase in winter occurrence of ~3 days (not robust at 90%). Group 2, associated with weaker Beaufort High features, does not show a prominent decrease (~1 day). Weak low pressure patterns in Group 3 also do not change drastically, increasing by ~1 day in winter. Spring shows the fewest frequency changes and they can be described as being similar to the summer changes but muted. Group 5 increases in frequency by ~4 days at the expense of all other patterns, except Group 4.

In order to investigate the linkages between synoptic activity and sea ice variability, correlations between CCSM4 20th and 21st century frequencies of occurrence for grouped patterns and year-to-year changes in September ice extent (for each respective model experiment) were calculated. They are compared in order to examine changing responsiveness of Arctic sea as the ice cover decreases. Correlations between 20th century SOM group frequencies and CCSM4 20th century Ensemble #6 year-to-year ΔSIE, shown in Table 5.5 are not as prominent as in the observations (Table 4.2). The correlations are coherent, however. For example, broad high pressure patterns present in Group 0 and stormy patterns with pressure gradients conducive to warm air advection in Group 1 correlate negatively to year-to-year ΔSIE in all seasons (although not statistically significant at 90%), up to -0.29 for Group 0 during winter. These findings are consistent with the importance of broad high pressures found to be important in the observations (Table 4.2).

Group 5 (from Figure 5.43) shows the only statistically significant correlation (at 95%) during winter and spring of 0.38. (Note that these correlations are only identical at two significant figures.) The mean winter occurrences of this group are relatively small (~4 days annually during winter), signaling that the correlation may be spurious. The spring correlation is more intuitive, as it is consistent with the finding from Screen et al. (2011) that late spring-early summer central Arctic storminess is linked to year-to-year ice gain through physical mechanisms, such as weakening the Transpolar Drift Stream. Group 2 correlates to year-to-year ice extent in spring (AMJ). This pattern is consistent with shuttling ice towards the Fram Strait. This group is somewhat similar to the "Beaufort Highs/Eurasian Lows" group in the ERA-Interim Master SOM (Figure 3.2), although weaker (as discussed earlier). The summer season shows the overall weakest correlations, likely due to the models issues in simulating the Beaufort High-type patterns important to ice motion (see Jahn et al. (2011)). It is interesting that the only robust correlations are for a group that is linked to sea ice gain. This hints that other processes or variables are dominating the ice loss, such as temperature. Also, CCSM4 is better able to simulate low pressure features over the central Arctic, associated with ice gain (Screen et al. (2011)), so it is not surprising that synoptic-ice linkages would be more robust with low pressure patterns.

Table 5.6 shows correlations between CCSM4 21st century group frequencies of occurrence and 21st century Ensemble #6 year-to-year ΔSIE. Overall, correlations are rather weak. This is likely due 1) little year-to-year ice variability in September in a future climate (Figure 5.45) and 2) to the ice variability being dominated by thermodynamic forcing, as opposed to synoptic activity (Holland and Stroeve (2011)). Correlations are no longer coherent within a group (i.e., correlations for a given group are not of the same sign for all seasons). For example, Group 5

exhibits negative correlations in summer and fall (of year N and year N-1, respectively). This suggests that the ice is no longer coherently responsive to the synoptic setup. This group's correlations are nearly zero for winter and spring, the seasons during which they were prominent in the 20th century. This is not surprising as Holland and Stroeve (2011) show that in the 21st century CCSM4 climate, correlations between Arctic basin temperature and September sea ice concentration strengthen relative to the 20th century correlations, while correlations to SLP weaken. Summer correlations have overall become stronger relative to the 20th century. For example, Group 0 is linked to ice loss at a correlation of -0.23 (not robust at 90% statistical significance). The most prominent changes are in fall (for grouped patterns occurring the year previous to the year-to-year ΔSIE). The only statistically significant robust correlation is during Fall for Group 2 and is correlated at 0.37 (statistically significant at 95%). Considering the one-year lag, the fall correlations are assumed to be spurious since the frequencies of occurrence are small (<1 day annually) on average.

These findings highlight that predicting the pressure patterns important for sea ice motion are integral to capturing synoptic-ice variability relationships. Considering that correlations were less robust than in ERA-Interim, this suggests that many tools should be used in sea ice projections, such as dynamical tools (models) and other statistical tools. This is especially true considering that CCSM4 captures the overall seasonality of ERA-Interim but exhibits biases in the frequencies of occurrence. Other aspects of the ice state should also be studied in order to tap into possible predictability, such as winter ice-synoptic relationships and studying regional ice change (along with pan-Arctic changes). Studying regional changes is particularly important since September ice trends are not uniform in all Arctic sea basins (e.g., Beaufort versus Bering Seas), and ice loss in the 21st century is also not expected to be uniform (Figure

5.47, taken and adapted from Deser et al. (2010b), Figure 1a). Other time slices, such as the mid-twenty first century and events during which drastic ice loss or gain occur, should also be studied within CCSM4 to quantify the atmosphere-ice relationships discussed earlier hold.

CCSM4 has been shown to reasonably capture the Arctic present-day climate but has a low pressure bias. This under-simulation of high pressure patterns, such as "High Pressure Bridges", "Beaufort Highs/Eurasian Lows" groups, contributes to the negative SLP bias. In observational data, antecedent seasonal frequencies of these patterns are linked to observed interannual ice variability. The model is missing these prominent linkages that would provide modest amounts of interannual September ice predictability. Accounting for these pressure biases does provide more prominent (but not robust) correlations to ice variability (e.g., in the case of the high pressure patterns and the "Eurasian Highs/Icelandic-Aleutian Lows" group), suggesting that the model can capture atmosphere-ice linkages when the synoptic atmospheric circulation is correctly simulated. Teleconnection patterns linked to ice variability (the AO, NAO, and AD) are shifted in the model, with too much interannual variability. This signals the need for further investigation into the shortcomings of GCMs in simulating large-scale modes of atmospheric variability and the shortcomings' roles in producing ice loss trends matching more closely to observations (refer to Stroeve et al. (2012)).

In the late 21st century, low pressures are projected to drastically increase by approximately 24% (15 days) in summer and 16% (5 days) in fall, with implications for coastal erosion and ocean navigation. The Arctic is essentially ice free in September for most of the late-21st century and year-to-year ice variability is reduced, leading to weaker atmosphere-ice variability linkages and signaling that future research should identify observed atmosphere-ice linkages in transition seasons. For example, March ice extent in the 21st century is projected to be ~4

million km^2 less than observed (Figure 5.48) but will still be of concern to marine and private prospects in navigating the Arctic peripheral seas.

Figure 5.43: CCSM4 Master SOM

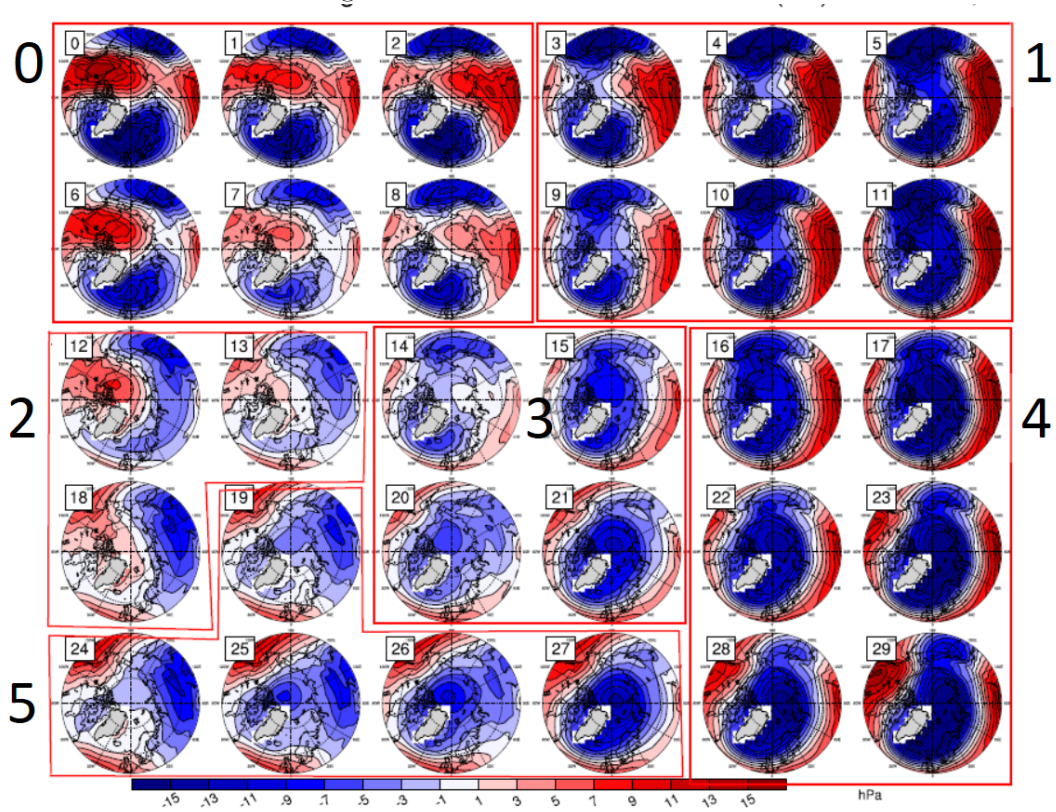

Master SOM of CCSM4 20th (1974-2005) and 21st (2069-2100) century daily sea-level pressure spatial anomalies (mb). Boxes and labels indicate groupings (Groups 0 to 5) discussed in the text.

Figure 5.44: Mean 20 and 21C Frequencies for the CCSM4 Master SOM

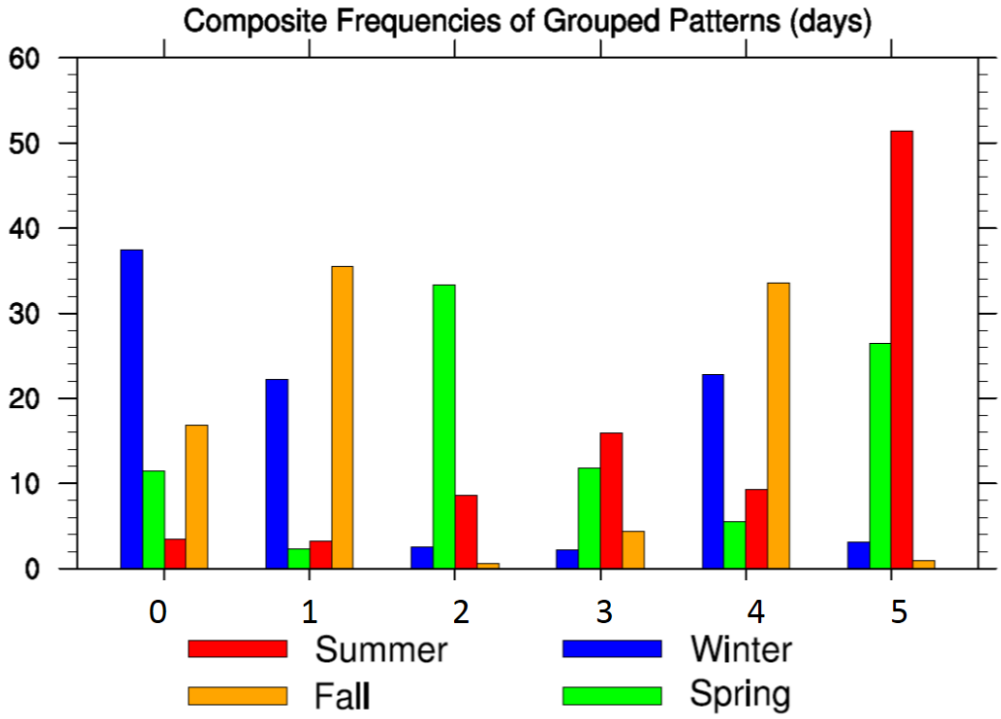

Seasonal composite frequencies (days) of grouped patterns (see Fig. 5.43) for JFM (blue), AMJ (green), JAS (red), and OND (orange) for the 20th (1974-2005) and 21st (2069-2100) centuries (Ensemble #6 experiments for each).

Table 5.3: 20th century CCSM4 group frequencies of occurrence

Group	Winter	Spring	Summer	Fall
0	36.8	14.8	3.5	18.0
1	23.3	3.7	2.1	33.7
2	2.0	32.2	13.1	0.7
3	1.8	13.0	16.6	5.6
4	25.0	7.3	6.2	32.8
5	1.2	20.0	50.6	1.3

Mean annual 20th century frequencies of occurrence (days) for each group from the CCSM4 Master SOM (Figure 5.43).

Figure 5.45: CCSM4 ensemble member 6 sep ice extent

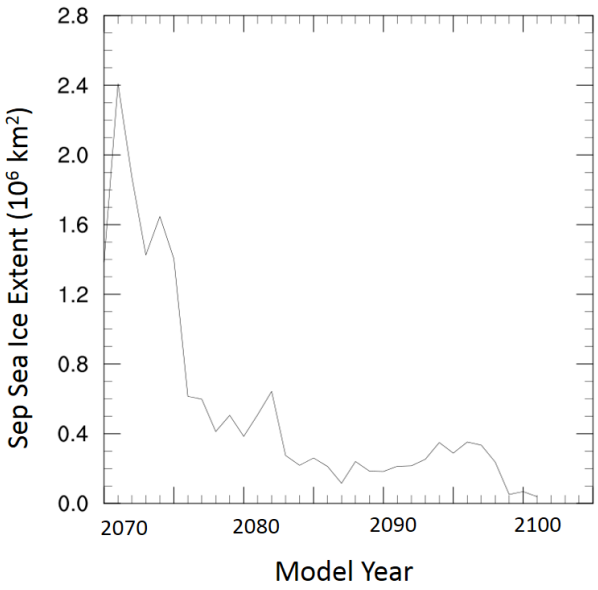

Time series of September pan-Arctic sea ice extent (10^6 km^2) from CCSM4 Ensemble #6 from model year 2069 to 2100. Sea ice extent was calculated using areas with 15% or more of modeled sea ice concentration.

Table 5.4: 21st century CCSM4 group frequencies of occurrence

Group	Winter	Spring	Summer	Fall
0	36.7	14.6	2.2	11.9
1	26.6	2.0	1.2	34.1
2	1.6	31.7	8.3	0.7
3	2.2	11.0	12.6	5.8
4	19.8	8.1	5.1	38.0
5	3.1	23.6	62.5	1.5

Mean annual 21st century frequencies of occurrence (days) for each group from the CCSM4 Master SOM (Figure 5.43).

Figure 5.46: Mean frequency of occurrence composite differences: 21C minus 20C

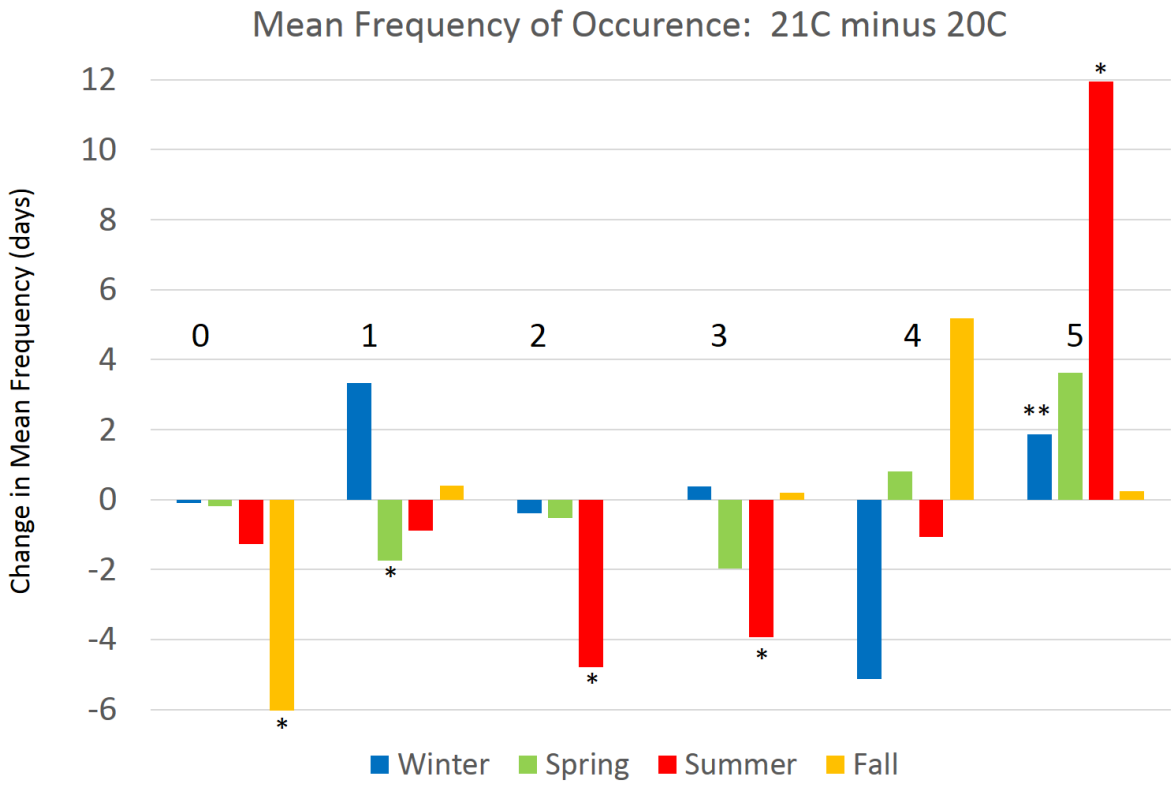

Composite differences (days) between 21st and 20th century mean annual frequencies of occurrence (21C minus 20C) for grouped patterns from Figure 5.43. Colors indicate season: JFM (blue), AMJ (green), JAS (red), and OND (orange). One asterisk (**) indicates statistical significance at 90% (95%) or greater.

Table 5.5: 20th century SOM-ice correlations computed from CCSM4 Master SOM

	Season			
Group	Winter	Spring	Summer	Fall
0	-0.22	-0.29	-0.15	-0.28
1	-0.26	-0.16	-0.16	-0.1
2	0.03	-0.25	-0.05	0.04
3	0.18	0.17	0.08	0.02
4	0.29	0.15	0.18	0.25
5	**0.38****	**0.38****	0.02	0.02

Correlations between 20th century annual frequencies and year-to-year change in September ice extent. Bold (**) indicates statistical significance equal to or greater than 90% (95%).

Table 5.6: 21st century SOM-ice correlations computed from CCSM4 Master SOM

	Winter	Spring	Summer	Fall
0	0	-0.04	-0.23	0.18
1	0.1	-0.22	-0.19	0.03
2	0.14	0.12	0.03	**0.37****
3	-0.08	-0.01	-0.02	0.2
4	-0.11	-0.19	0.26	-0.19
5	0.02	0.03	-0.01	-0.21

Correlations between 21st century annual frequencies and year-to-year change in September ice extent. Bold (**) indicates statistical significance equal to or greater than 90% (95%).

Figure 5.47: MA and MJ Sea Ice Concentrations 1980-99 and 2080-2099

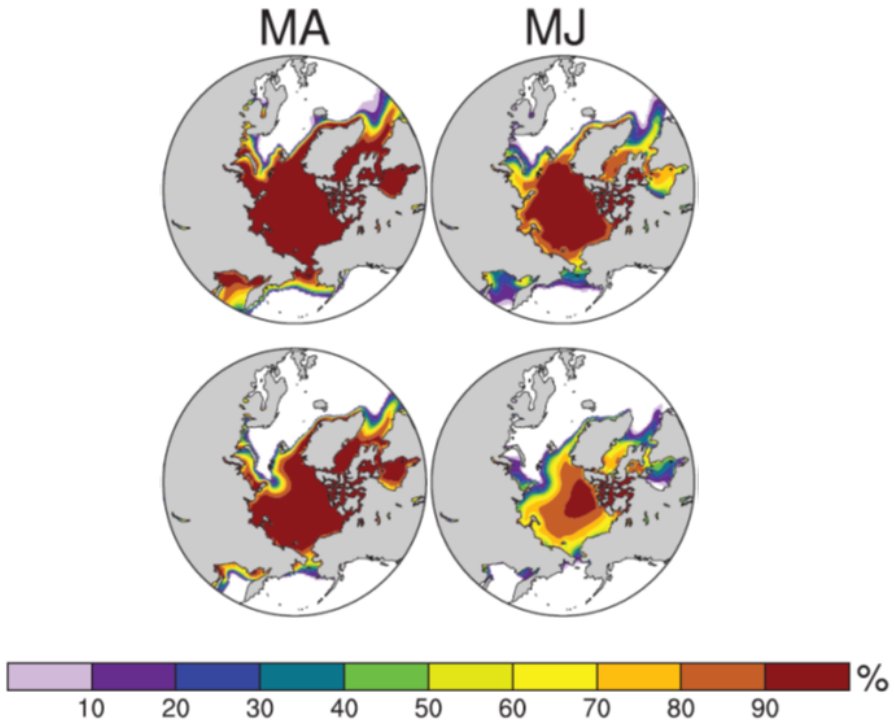

Ice concentrations (%) for 1980-1999 (top) and 2080-2099 (bottom) for March and April (MA) and May and June (MJ). Taken and adapted from Figure 1(a) of Deser et al. (2010b).

Figure 5.48: CCSM4 ensemble member 6 Mar ice extent

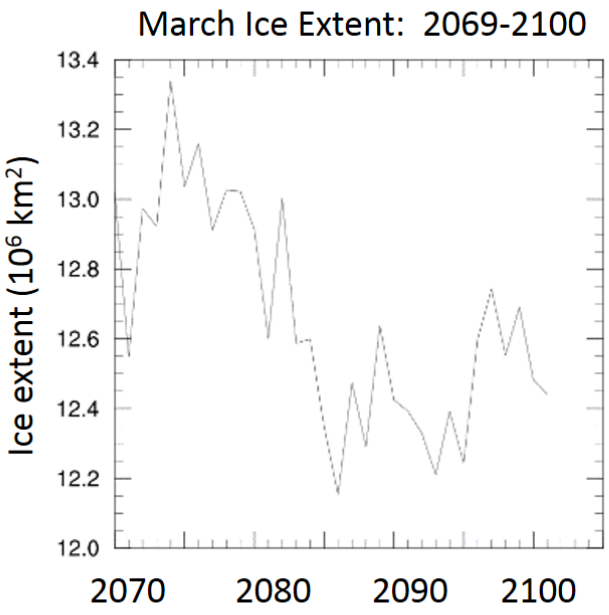

Time series of March pan-Arctic sea ice extent (10^6 km^2) from CCSM4 Ensemble #6 from model year 2060 to 2100. Sea ice extent was calculated using areas with 15% or more of modeled sea ice concentration.

Chapter 6

Conclusions

The SOM analysis was employed to provide a framework for a diagnosis of synoptic patterns that play a role in sea ice variability in both observations and a frequently used model n the Arctic, CCSM4. This was investigated by (1) correlating the time series of synoptic patterns and groups within the Master SOM with various sea ice metrics to examine what role synoptic patterns play in preconditioning ice, (2) analyzing trends in time series of recent observed synoptic patterns, (3) investigating biases in the CCSM4 present-day climate, and (4) comparing frequencies in present and future climates. The main findings are summarized below:

- SOMs can identify observed synoptic patterns that correlate better to time series of sea ice metrics than do time series of modes of atmospheric circulation variability, such as the NAO, AO, and AD.

- Observed synoptic patterns containing Beaufort Highs are increasing in frequency in spring and summer by 3 days (at 90% confidence) and 1.8 days per decade, respectively, and their spring frequencies are linked to ice loss at a 99% statistically significant

correlation of -0.50.

- Winter “High Pressure Bridges” patterns in ERA-Interim show a strong relationship to sea ice loss through their role in advecting thick ice through the Fram Strait during winter, preconditioning ice for loss the following summer and are increasing in frequency (although not statistically significant at 90% confidence) and intensity during winter.

- Warm air advection associated with observed Icelandic lows (in the “Eurasian Highs-Icelandic/Aleutian Lows” group) prior to and during the melt season favors year-to-year decreases of late-summer sea ice.

- The CCSM4 present-day climate exhibits a low pressure bias and undersimulates high pressure patterns important for observed ice loss, such as the "High Pressure Bridges" group by approximately 6 and 10 days during winter and fall, respectively.

- These biases are also portrayed by producing a higher-than-observed frequency of strong storm track features (e.g., "Icelandic Lows/Fram Strait Outflow" patterns by approximately 20 days during the fall season); the model also oversimulates "Weak Features" patterns in all seasons by up to 12 days in the summer season. These patterns were not shown to be prominently linked to observed ice variability.

- When SLP bias-adjustments are applied to CCSM4 20th century daily SLP fields, atmosphere -ice correlations more prominent (and closer to observed linkages), suggesting that the model can capture atmosphere-ice linkages, at least partially, if the model simulates the frequencies of important patterns correctly.

- CCSM4 overall captures large-scale atmospheric teleconnection patterns over the Arctic,

such as the AO, NAO, and AD, but spatial shifts are apparent that affect ice motion, and the model displays enhanced interannual variability of these teleconnection patterns relative to observations.

- The CCSM4 21st century climate shows a prominent increase in strong low pressure patterns associated with ice loss, with an increase in strong central Arctic low patterns (Groups 4 and 5) during fall and summer by 24% and 15% relative to the present-day CCSM4 climate.

- The CCSM4 21st century atmosphere-ice dynamical linkages are overall weaker than the 20th century CCSM4 linkages, due to the absence of ice to provide prominent variability in an ice-free Arctic.

The SOM analysis and time series associated with synoptic patterns provide a means to quantify the relationships between synoptic variability and rapidly thinning sea ice. Because SOM patterns of antecedent seasons correlate with ΔSIE, the findings obtained here imply predictability of large-scale ice loss/gain over seasonal timescales and could add to already available methods of atmospheric predictors of sea ice variability (NRC (2012)). Moreover, the ice pack is thinning in all seasons, signaling that even winter and spring atmospheric circulation patterns are important in preconditioning the ice prior to the melt season.

Since linkages between synoptic activity and ΔSIE are weaker in CCSM4 than observations, model simulation of important features, such as high pressures over the Beaufort in winter should be investigated and improved. When model biases were corrected for, patterns linked to ice loss, such as the "High Pressure Bridges" group and "Beaufort Highs/Eurasian Lows" patterns increase in frequency in most seasons and these patterns' correlations to interannual

ice variability also become more prominent. These findings suggest that a major cause of the weaker-than-observed atmosphere-ice coupling could be the undersimulation and spatial shifts of important SLP patterns, not just systemic biases in temperature and cloud production (although they are intrinsically linked to atmospheric synoptic activity), for example. Which issues dominate the weaker atmosphere-ice linkages dominate is worthy of further investigation: 1) the model not coupling wind forcing associated with synoptic activity to interannual ice variability, 2) the inability of the model to capture interannual atmospheric variability, or 3) systemic biases overwhelming the atmosphere-ice linkages.

An increase in low pressure patterns in the 21st century has implications for enhanced coastal inundation and erosion. Many Alaskan communities are already in the process of or planning relocation and are increasingly seeking information from the Arctic science community. Reducing biases in capturing Arctic synoptic activity is an important task for providing reasonable Arctic climate projections. As interannual variability is reduced in September in the late 21st century, wind-ice coupling in transition seasons should also be investigated.

Bibliography

Alexeev, V. A., Ivanov, V. V., Kwok, R., and Smedsrud, L. H. 2013. North atlantic warming and declining volume of arctic sea ice. *The Cryosphere Discussions*, 7(1):245–265.

Asplin, M. G., Lukovich, J. V., and Barber, D. G. 2009. Atmospheric forcing of the beaufort sea ice gyre: Surface pressure climatology and sea ice motion. *Journal of Geophysical Research: Oceans*, 114(C1):C00A06.

Bengtsson, L., Hodges, K. I., and Roeckner, E. 2006. Storm tracks and climate change. *Journal of Climate*, 19(15):3518–3543.

Bitz, C. M., Fyfe, J. C., and Flato, G. M. 2002. Sea ice response to wind forcing from amip models. *Journal of Climate*, 15(5):522–536.

Bromwich, D. H., Fogt, R. L., Hodges, K. I., and Walsh, J. E. 2007. A tropospheric assessment of the era-40, ncep, and jra-25 global reanalyses in the polar regions. *Journal of Geophysical Research: Atmospheres*, 112(D10):D10111.

Cassano, J. J., Uotila, P., and Lynch, A. 2006. Changes in synoptic weather patterns in the polar regions in the twentieth and twenty-first centuries, part 1: Arctic. *International Journal of Climatology*, 26(8):1027–1049.

Cavazos, T. 1999. Large-scale circulation anomalies conducive to extreme precipitation events and derivation of daily rainfall in northeastern Mexico and southeastern Texas. *Journal of Climate*, 12(5):1506–1523.

de Boer, G., Chapman, W., Kay, J. E., Medeiros, B., Shupe, M. D., Vavrus, S., and Walsh, J. 2011. A characterization of the present-day arctic atmosphere in CCSM4. *Journal of Climate*, 25(8):2676–2695.

Deser, C., Phillips, A., Bourdette, V., and Teng, H. 2010a. Uncertainty in climate change projections: the role of internal variability. *Climate Dynamics*, pages 1–20.

Deser, C., Tomas, R., Alexander, M., and Lawrence, D. 2010b. The seasonal atmospheric response to projected arctic sea ice loss in the late twenty-first century. *Journal of Climate*, 23(2):333–351.

Eisenman, I., Untersteiner, N., and Wettlaufer, J. 2007. On the reliability of simulated arctic sea ice in global climate models. *Geophysical Research Letters*, 34(10).

Fetterer, F., Knowles, K., Meier, W., and Savoie, M. 2002, updated daily. Sea Ice Index. 1979-2010, edited. Boulder, Colorado, USA. National Snow and Ice Data Center.

Francis, J. A. and Hunter, E. 2007. Changes in the fabric of the arctic's greenhouse blanket. *Environmental Research Letters*, 2(4):045011.

Francis, J. A., Hunter, E., Key, J. R., and Wang, X. 2005. Clues to variability in arctic minimum sea ice extent. *Geophysical Research Letters*, 32(21):L21501.

Gent, P. R., Danabasoglu, G., Donner, L. J., Holland, M. M., Hunke, E. C., Jayne, S. R., Lawrence, D. M., Neale, R. B., Rasch, P. J., Vertenstein, M., Worley, P. H., Yang, Z.-L.,

and Zhang, M. 2011. The Community Climate System Model Version 4. *Journal of Climate*, 24(19):4973–4991.

Gleicher, K. J., Walsh, J. E., and Chapman, W. L. 2011. A vorticity-based analysis of the spatial and temporal characteristics of the beaufort anticyclone. *Journal of Geophysical Research: Atmospheres*, 116(D18):D18115.

Hewitson, B. C. and Crane, R. G. 2002. Self-organizing maps: applications to synoptic climatology. *Climate Research*, 22(1):13–26.

Higgins, M. E. and Cassano, J. J. 2009. Impacts of reduced sea ice on winter arctic atmospheric circulation, precipitation, and temperature. *J. Geophys. Res.*, 114(D16):D16107.

Holland, M. M. and Stroeve, J. 2011. Changing seasonal sea ice predictor relationships in a changing arctic climate. *Geophysical Research Letters*, 38(18):n/a–n/a.

Hurrell, J. W. 1995. Decadal trends in the north atlantic oscillation. *Science*, 269:676–679.

Jahn, A., Sterling, K., Holland, M. M., Kay, J. E., Maslanik, J. A., Bitz, C. M., Bailey, D. A., Stroeve, J., Hunke, E. C., Lipscomb, W. H., and Pollak, D. A. 2011. Late-twentieth-century simulation of arctic sea ice and ocean properties in the CCSM4. *Journal of Climate*, 25(5):1431–1452.

Kay, J. E., Holland, M. M., and Jahn, A. 2011. Inter-annual to multi-decadal arctic sea ice extent trends in a warming world. *Geophysical Research Letters*, 38(15):L15708.

Kohonen, T. 2001. *Self-Organizing Maps*, volume 30 of *Springer series in information sciences*. Springer.

Kwok, R. 2009. Outflow of Arctic Ocean Sea Ice into the Greenland and Barents Seas: 1979-2007. *Journal of Climate*, 22(9):2438–2457.

Kwok, R. and Rothrock, D. A. 2009. Decline in arctic sea ice thickness from submarine and ICESat records: 1958-2008. *Geophysical Research Letters*, 36(15):L15501.

Laxon, S. W., Giles, K. A., Ridout, A. L., Wingham, D. J., Willatt, R., Cullen, R., Kwok, R., Schweiger, A., Zhang, J., Haas, C., Hendricks, S., Krishfield, R., Kurtz, N., Farrell, S., and Davidson, M. 2013. CryoSat-2 estimates of Arctic sea ice thickness and volume. *Geophysical Research Letters*, 40(4):732–737.

L'Heureux, M. L., Kumar, A., Bell, G. D., Halpert, M. S., and Higgins, R. W. 2008. Role of the Pacific-North American (PNA) pattern in the 2007 Arctic sea ice decline. *Geophysical Research Letters*, 35(20):L20701.

Maslanik, J., Stroeve, J., Fowler, C., and Emery, W. 2011. Distribution and trends in arctic sea ice age through spring 2011. *Geophysical Research Letters*, 38(13):L13502.

McCabe, G. J., Clark, M. P., and Serreze, M. C. 2001. Trends in northern hemisphere surface cyclone frequency and intensity. *Journal of Climate*, 14(12):2763–2768.

NRC 2012. *Seasonal-to-Decadal Predictions of Arctic Sea Ice: Challenges and Strategies*. The National Academies Press.

Ogi, M. and Wallace, J. M. 2012. The role of summer surface wind anomalies in the summer arctic sea ice extent in 2010 and 2011. *Geophysical Research Letters*, 39(9):L09704.

Ogi, M., Yamazaki, K., and Wallace, J. M. 2010. Influence of winter and summer surface wind anomalies on summer arctic sea ice extent. *Geophysical Research Letters*, 37.

Overland, J. E., Francis, J. A., Hanna, E., and Wang, M. 2012. The recent shift in early summer arctic atmospheric circulation. *Geophysical Research Letters*, 39(19):L19804.

Rampal, P., Weiss, J., and Marsan, D. 2009. Positive trend in the mean speed and deformation rate of arctic sea ice, 1979-2007. *Journal of Geophysical Research: Oceans*, 114(C5):C05013.

Reusch, D. B., Alley, R. B., and Hewitson, B. C. 2005. Relative performance of self-organizing maps and principal component analysis in pattern extraction from synthetic climatological data. *Polar Geography*, 29(3):188–212.

Rigor, I. G., Wallace, J. M., and Colony, R. L. 2002. Response of sea ice to the arctic oscillation. *Journal of Climate*, 15(18):2648–2663.

Sammon Jr, J. W. 1969. A nonlinear mapping for data structure analysis. *Computers, IEEE Transactions on*, 100(5):401–409.

Screen, J. A., Simmonds, I., and Keay, K. 2011. Dramatic interannual changes of perennial arctic sea ice linked to abnormal summer storm activity. *Journal of Geophysical Research: Atmospheres*, 116(D15):D15105.

Serreze, M. and Barry, R. 2005. *The Arctic climate system*. Cambridge Atmospheric and Space Science Series. Cambridge.

Serreze, M. C. and Barrett, A. P. 2010. Characteristics of the Beaufort Sea High. *Journal of Climate*, 24(1):159–182.

Serreze, M. C., Lynch, A. H., and Clark, M. P. 2001. The Arctic frontal zone as seen in the NCEP-NCAR Reanalysis. *Journal of Climate*, 14(7):1550–1567.

Shimada, K., Kamoshida, T., Itoh, M., Nishino, S., Carmack, E., McLaughlin, F., Zimmermann, S., and Proshutinsky, A. 2006. Pacific ocean inflow: Influence on catastrophic reduction of sea ice cover in the arctic ocean. *Geophysical Research Letters*, 33(8):L08605.

Simmonds, I. and Keay, K. 2009. Extraordinary september arctic sea ice reductions and their relationships with storm behavior over 1979-2008. *Geophysical Research Letters*, 36(19):L19715.

Stroeve, J. C., Kattsov, V., Barrett, A., Serreze, M., Pavlova, T., Holland, M., and Meier, W. N. 2012. Trends in Arctic sea ice extent from CMIP5, CMIP3 and observations. *Geophysical Research Letters*, 39(16):L16502.

Stroeve, J. C., Maslanik, J., Serreze, M. C., Rigor, I., Meier, W., and Fowler, C. 2011. Sea ice response to an extreme negative phase of the Arctic Oscillation during winter 2009/2010. *Geophysical Research Letters*, 38(2):L02502.

Thompson, D. W. and Wallace, J. M. 1998. The Arctic Oscillation signature in the wintertime geopotential height and temperature fields. *Geophysical Research Letters*, 25(9):1297–1300.

Vavrus, S. and Waliser, D. 2008. An improved parameterization for simulating Arctic cloud amount in the CCSM3 climate model. *Journal of Climate*, 21(21).

Vavrus, S. J., Holland, M. M., Jahn, A., Bailey, D. A., and Blazey, B. A. 2011. Twenty-first-century arctic climate change in CCSM4. *Journal of Climate*, 25(8):2696–2710.

Walsh, J. E., Chapman, W. L., and Shy, T. L. 1996. Recent decrease of sea level pressure in the central arctic. *Journal of Climate*, 9(2):480–486.

Wu, B., Overland, J. E., and Arrigo, R. 2012. Anomalous arctic surface wind patterns and their impacts on september sea ice minima and trend. *Tellus A*, 64.

Wu, B., Wang, J., and Walsh, J. E. 2006. Dipole anomaly in the winter arctic atmosphere and its association with sea ice motion. *Journal of Climate*, 19(2):210–225.

Zhang, X., Walsh, J. E., Zhang, J., Bhatt, U. S., and Ikeda, M. 2004. Climatology and interannual variability of arctic cyclone activity: 1948 - 2002. *Journal of Climate*, 17(12):2300–2317.